AD NUMBER
AD526738
CLASSIFICATION CHANGES
TO: **UNCLASSIFIED**
FROM: **CONFIDENTIAL**
LIMITATION CHANGES
TO: **Approved for public release; distribution is unlimited.**
FROM: **Distribution authorized to U.S. Gov't. agencies only; Test and Evaluation; MAY 1973. Other requests shall be referred to Rome Air Development Center, Griffiss AFB, NY.**
AUTHORITY
31 May 1985, DoDD 5200.10; RADC ltr 3 Dec 1979

RADC-TR-73-136
Final Technical Report
May 1973

OPTICAL PROCESSING OF ROTATING-OBJECT RADAR DATA USING A POLAR RECORDING FORMAT (U)

Environmental Research Institute of Michigan

Rome Air Development Center
Air Force Systems Command
Griffiss Air Force Base, New York

A classified appendix has been inserted in the body of this report and can be found on pages 41, 41A, 41B, and 41C. The applicable figures are A-1 and A-2. No attempt was made to renumber the pages or to change the figure numbers because the type font used in the original reproducible copy is not available at RADC.

OPTICAL PROCESSING OF ROTATING-OBJECT RADAR DATA USING A POLAR RECORDING FORMAT (U)

J. L. Walker
W. G. Carrara
I. Cindrich

Environmental Research Institute of Michigan

FOREWORD

This report was prepared by the Radar and Optics Division of the Environmental Research Institute of Michigan for the Rome Air Development Center under Contract F30602-72-C-0062, Job Order No. 45060176. The period of the contract was 1 February 1972 to 1 February 1973. The RADC Project Monitor was K. Stiefvater/OCTE.

The Principal Investigator on this project was J. L. Walker. Section 1-5 of this report were written by J. L. Walker and Section 6 by I. Cindrich. W. G. Carrara played a significant role in much of the work reported here. This work has also benefited from the critical review and suggestions of Dr. J. S. Zelenka.

The Environmental Research Institute of Michigan number for this report is 191400-1-F.

This report contains no classified information extracted from other classified documents.

This technical report has been reviewed and is approved.

Approved: Kenneth Stiefvater
KENNETH STIEFVATER
Project Engineer

Approved: William T. Pope
WILLIAM T. POPE
Assistant Chief
Surveillance and
Control Division

FOR THE COMMANDER: John P. Huss

JOHN P. HUSS
Acting Chief, Plans Office

ABSTRACT

A new optical processing technique for producing fine resolution radar images of rotating objects has been investigated. The technique involves optically recording the radar data in an appropriate polar format to eliminate the usual image degradation caused by motion of object points through resolution cells.

Experiments were performed in which X-band radar data from various test objects placed on a rotating platform were recorded on photographic film in a polar format and optically processed. The resulting imagery demonstrated the fine resolution and object-shape recognition capability afforded by the use of the polar recording format.

The feasibility of using thermoplastic as a real-time storage medium for radar data was investigated. The thermoplastic data storage technique was shown to have sound potential for use in a real-time optical processing system for satellite imaging applications.

CONTENTS

FIGURES

Evaluation Memo on Final Report

Project No. 45060176

Contract: F30602-72-C-0062

Title: Optical Processing of Rotating-Object Radar Data Using A Polar Recording Format

Contractor: Radar and Optics Division/Environmental Res. Inst. of Michigan Box 618, Ann Arbor, MI 48107

1. A technique which has been investigated in recent years (RADC contracts AF30602-4208 and F30602-68-C-0004) for optical processor for wideband radar imaging of various types of rotating bodies is based on a range-doppler analysis of the reflected signal from such objects. Good range resolution is obtained by transmitting a wide bandwidth signal and the variation in doppler velocity across the rotating object permits one to also obtain cross range resolution by means of synthetic aperture processing.

2. A major limitation of the optical range doppler system, discovered in the previous work, was caused by the motion of the objects reflecting points through resolution cells within the processing interval. In the present program this has been overcome by storing the radar returns in a polar format (instead of the usual rectangular format) and optically taking the Fourier transform. This technique allows one to coherently process rotating object data over large angular intervals with no image degradation due to motion through the resolution cells. Imagery of test objects placed on a rotating platform demonstrated that resolution of nearly one radar wavelength could be achieved which produces excellent shape recognition.

3. The real time feature of the processor is accomplished by replacing the usual used photographic film with a thermoplastic electroptic transducer. This is accomplished by writing radar video on the thermoplastic disc with an electron gun. The plastic is heated prior to the impinging of the electron beam which causes it to deform, producing a stored signal. Coherent light is then passed through a lens system and the plastic disc to produce an image. The thermoplastic data storage technique has been shown to have a sound potential from the results of this program. Experiments have shown that video bandwidth of at least 10 MHz can be stored with good optical quality over apertures containing 400 X 400 resolvable recorded elements.

4. The program supports TPO-18 "Electromagnetic Generation, Amplification and Control" and TPO-6 "Space Surveillance", referenced in RADC Technology Plan dated June 72. The intended use of this technique is to provide a real time optical processor to produce imagery of satellites from data supplied from the Floyd Wideband Pulse Compression Radar.

Kenneth Stiefvater

KENNETH STIEFVATER
RADC Project Engineer

OPTICAL PROCESSING OF ROTATING-OBJECT RADAR DATA USING A POLAR RECORDING FORMAT

1 INTRODUCTION

A well known technique for producing radar images of rotating objects involves analyzing the signal reflected from these objects in terms of range-delay and Doppler frequency [1, 2, 3, 4]. One important application of this technique is in satellite-object identification, including size and shape estimation.

The resolution achievable with the usual first-order range-Doppler imaging systems for rotating objects is limited by the motion of object points during a coherent processing time interval [5]. The resolution must be sufficiently coarse that points on the object move less than one resolution cell during the processing interval. For an object with diameter, D, and a radar wavelength, λ, the achievable resolution is on the order of $\sqrt{\lambda D/2}$. Under previous RADC contracts AF30(602)-4208 and F30602-68-C-0004, optical processing of rotating-object radar data for satellite imaging applications was investigated and some techniques for partial compensation of motion through resolution cells were devised [6, 7].

This report presents the results of an investigation of a new technique which allows one to optically process rotating-object radar data over large intervals and thereby obtain very fine resolution imagery not limited by motion through resolution cells. The technique involves optically recording the radar data in a polar format and then processing the resulting spatial signal by performing a two-dimensional Fourier transformation.

The basic polar recording format concept was originally derived to improve the resolution performance of airborne synthetic aperture radars used for terrain imaging. The work reported here was directed toward application of the concept to the problem of satellite imaging.

A breadboard, polar format, film recorder was constructed and used in conjunction with the ERIM Rotating Platform Radar Facility to investigate experimentally the polar recording format approach in terms of improving resolution and object shape detectability. Examples of imagery for various test objects placed on the rotating platform are presented in Section 4.

The use of ordinary photographic film as the storage medium in an optical processing system prohibits any real-time applications. Therefore, part of the technical effort described in this report was devoted to investigating the feasibility of using a thermoplastic electro-optic transducer as part of a real-time optical processor. Primary emphasis was placed on evaluating the performance of thermoplastic by using test recording parameters compatible with satellite imaging applications.

2
REVIEW OF ROTATING-OBJECT IMAGING

As background for the remainder of the report, we briefly review in this section the basic concept of range-Doppler imaging, the problem of motion through resolution cells, and the polar recording format approach. For simplicity, we consider here the two-dimensional object/radar geometry shown in Fig. 1. Section 3 gives a more detailed description of rotating-object imaging and treats three-dimensional effects.

If the initial location of a point scatterer on the rotating object shown in Fig. 1 is (x_o, y_o) then at time t the distance r from a distant $\left(\rho_a^2 >> x_o^2 + y_o^2\right)$ radar antenna to the point is approximately

$$r = \rho_a + x_o \sin \Omega t + y_o \cos \Omega t \tag{1}$$

where Ω is the rotation rate.

The Doppler frequency f_d of the return radar signal is

$$f_d = \frac{2}{\lambda}\left(\frac{dr}{dt}\right) = \left(\frac{2x_o\Omega}{\lambda}\right)\cos \Omega t - \left(\frac{2y_o\Omega}{\lambda}\right)\sin \Omega t \tag{2}$$

where λ is the radar wavelength.

If we process the radar data over a very small time interval, Eqs. (1) and (2) can be approximated as

$$r = \rho_a + y_o \tag{3}$$

$$f_d = \frac{2x_o\Omega}{\lambda} \tag{4}$$

Therefore, by analyzing the return radar signal in terms of range-delay and Doppler frequency, the position of the point scatterer (x_o, y_o) can be determined. Fine range resolution is obtained by transmitting a wideband signal, whereas Doppler frequency resolution, and hence cross-range resolution, is inversely proportional to the length of the processing time interval.

The presence of the object rotation rate, Ω, in Eq. (4) implies that in order to obtain a properly scaled x, y image of the object, the magnitude of Ω must be known. Most techniques for estimating the rotation rate depend on a priori knowledge and an analysis of periodicities in the radar signal level.

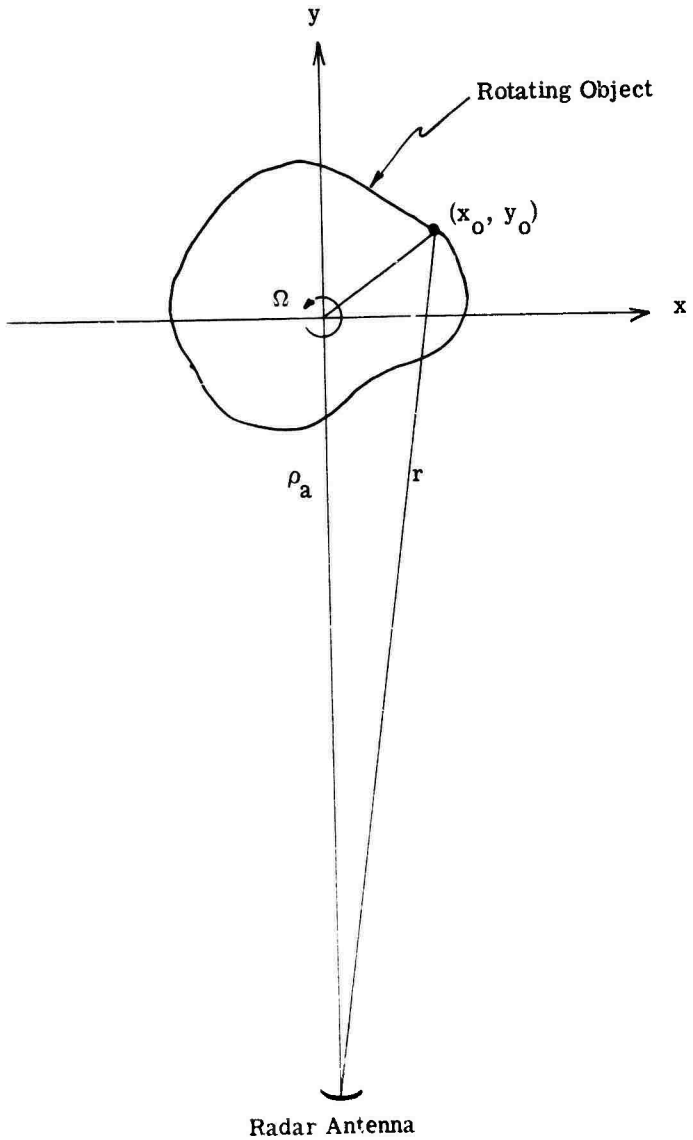

FIGURE 1. TWO-DIMENSIONAL RADAR/OBJECT GEOMETRY

Another implicit assumption here is that the distance ρ_a from the radar antenna to the center of the object is constant and known. (In an actual satellite imaging case, of course, ρ_a is a function of time.) The effects of time-varying gross range and range rate as the satellite moves along its trajectory must be removed in the radar receiver and/or processor.

Since the Doppler frequency resolution Δf_d varies inversely with the processing time interval T, we see from Eq. (4) that the cross-range resolution Δx is

$$\Delta x = \frac{\lambda}{2\Delta\phi} \tag{5}$$

where $\Delta\phi = \Omega T$ and is the change in angle over which the object rotates during the processing time. Fine cross-range resolution implies that we process over a large $\Delta\phi$; however, Eqs. (1) and (2) indicate that both the range and Doppler frequency of a particular point scatterer can vary greatly over a large processing interval. This means that during a processing time interval sufficiently long to give the desired cross-range resolution, points on the rotating object may move through several resolution cells. The simple range-delay measurement and Doppler-frequency analysis (Fourier transform) type of processing implied by Eqs. (3) and (4) will result in severely degraded imagery for the large processing interval case.

As shown in Ref. [6], the phase errors caused by motion through resolution cells impose the following resolution limitations

$$(\Delta x)^2 > \frac{\lambda D_y}{2} \tag{6}$$

$$\Delta x \Delta y > \frac{\lambda D_x}{2} \tag{7}$$

where Δx is cross-range resolution

Δy is range resolution

D_y is object width in range, and

D_x is object width in cross-range

In order to obtain resolution finer than this, it is necessary to compensate for the changing range and Doppler frequency associated with each object point during the processing interval. The problem of motion through resolution cells—sometimes called range-walk and variable range rate—has been investigated under previous RADC contracts; some compensation techniques are described in Refs. [5, 6, 7] in the context of optical data processors.

In the usual optical implementation of a range-Doppler processing system, the radar video signal is first recorded on photographic film in a rectangular format. This is accomplished, as shown in Fig. 2(a), by properly intensity-modulating a line-scan CRT and imaging the trace onto a strip of translating film. If the radar transmits wide bandwidth linear FM pulses and if return signal is mixed with an appropriate linear FM reference signal, the resulting video signal for a single point scatterer is a simple CW pulse with a frequency proportional to the range of the point. The resulting film recording for this type of signal is shown in Fig. 2(b).

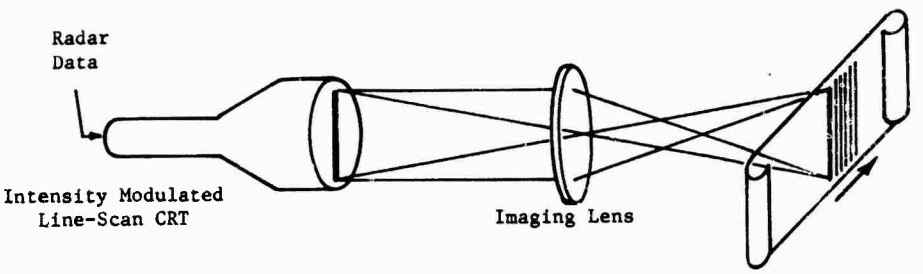

(a) Recorder

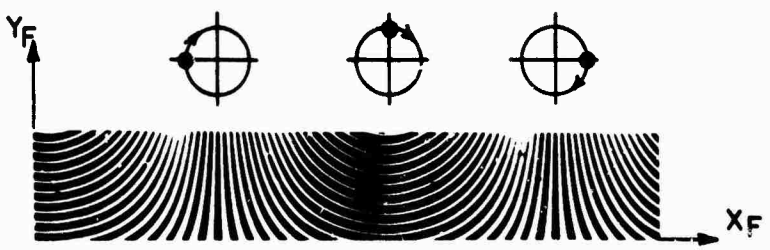

(b) Recorded Signal Corresponding to Point Scatterer on a Rotating Object

FIGURE 2. RECTANGULAR FORMAT RECORDING SYSTEM

Since both the range and Doppler frequency associated with a particular point on the rotating object vary sinusoidally with time as described in Eqs. (1) and (2), we see that the vertical (range) and horizontal (cross-range) spatial frequency components of the recorded modulation also vary sinusoidally. The three circular diagrams drawn above the recorded signal in Fig. 2(b) indicate three discrete positions of the point scatterer on a rotating object.

Over small regions of the recorded signal the modulation lines are approximately straight, therefore an optical two-dimensional Fourier transform will produce an image of the point scatterer. The curvature of these lines limits the useful size of the processing aperture, and hence the achievable resolution. This is the same limitation given by Eqs. (6) and (7).

The optical approach most often used in the past for partially compensating for motion through resolution cells is called sectional processing [6]. In sectional processing, somewhat larger processing apertures can be used and the effects of modulation line curvature [Fig. 2(b)] are reduced by properly adjusting the lenses in the optical processor. Since a different adjustment is required to optimize the resolution for each portion of the object, the final image must be produced by photographically summing individually processed image sections.

Under the present contract, we have investigated a new technique for eliminating the problem of motion through resolution cells. It involves storing the demodulated radar returns in a polar format by means of the recording scheme shown in Fig. 3(a). Here, instead of translating the recording film past a line-scan CRT as is done in the usual recorders, we cause the recording film to rotate at the object rotation rate Ω. The resulting recorded modulation for each point scatterer is a family of straight lines (a linear grating) as shown in Fig. 3(b). Thus the effects of motion through resolution cells are completely eliminated. Each point scatterer on the rotating object produces a grating type of recording with a spatial frequency and orientation determined by the initial coordinates (x_o, y_o) of the point. The total recorded signal for a complex rotating object consists of a coherent summation of a multiplicity of such gratings. Imagery of fine resolution can thus be obtained by Fourier transforming the recorded signal optically over very large apertures.

Examples of imagery obtained by using a polar recording format are given in Section 4, while a more detailed mathematical description of the polar format technique is presented in the next section.

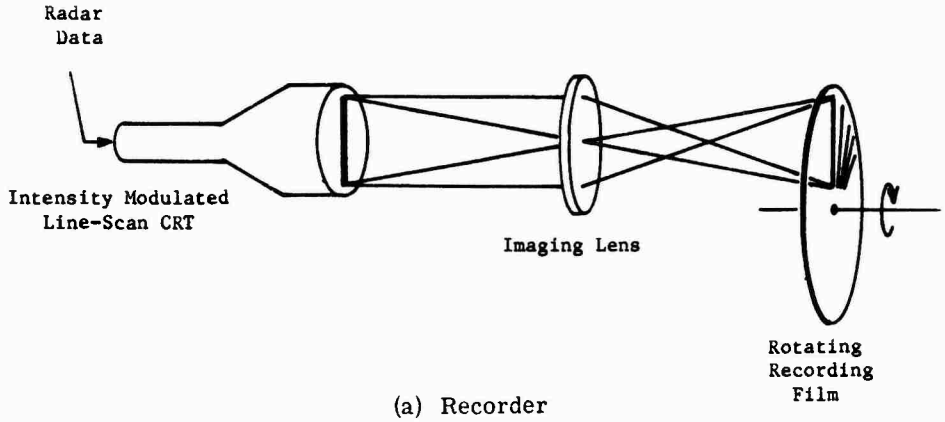

(a) Recorder

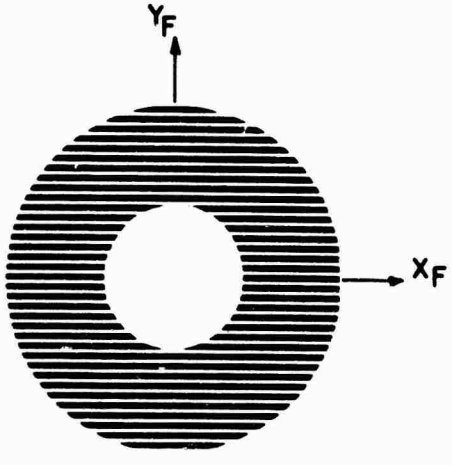

(b) Recorded Signal Corresponding to Point Scatterer on a Rotating Object

FIGURE 3. POLAR FORMAT RECORDING SYSTEM

3
MATHEMATICAL FORMULATION

This section presents a derivation of the polar recording format technique and discusses important image effects caused by the three-dimensional aspects of a rotating object.

Figure 4 shows the basic geometry under consideration here. Locations of the antenna and an arbitrary point on the three-dimensional rotating object are given in spherical coordinates as $(\rho_a, \theta_a, \phi_a)$ and $(\rho_o, \theta_o, \phi_o)$ respectively. The distance r from the radar antenna to an object point is

$$r = \left(\rho_a^2 + \rho_o^2 - 2\vec{\rho}_o \cdot \vec{\rho}_a\right)^{1/2} \tag{8}$$

where $\vec{\rho}_o$ and $\vec{\rho}_a$ are vectors defined in Fig. 4 and

$$\vec{\rho}_o \cdot \vec{\rho}_a = \rho_o \rho_a \left[\cos\theta_a \cos\theta_o + \sin\theta_a \sin\theta_o \cos(\phi_o - \phi_a)\right] \tag{9}$$

Using the binominal expansion, we can rewrite Eq. (8) as

$$r = \rho_a \left[1 + \frac{\rho_o^2 - 2\vec{\rho}_o \cdot \vec{\rho}_a}{2\rho_a^2} - \frac{1}{8}\left(\frac{\rho_o^2 - 2\vec{\rho}_o \cdot \vec{\rho}_a}{\rho_a^2}\right)^2 + \ldots\right] \tag{10}$$

Since for satellite imaging applications, the size of the object is much less than the range of the object from the antenna (that is, $\rho_o \ll \rho_a$), Eq. (9) can be approximated as follows:

$$r \approx \rho_a \left[1 - \frac{\vec{\rho}_o \cdot \vec{\rho}_a}{\rho_a^2}\right] \tag{11}$$

or using Eq. (9) we have

$$r \approx \rho_a - \rho_o \left[\cos\theta_a \cos\theta_o + \sin\theta_a \sin\theta_o \cos(\phi_o - \phi_a)\right] \tag{12}$$

In the physical situation the radar antenna is fixed while the object has both a rotational and translational motion. For convenience, we make the equivalent assumption here that the object is fixed and the antenna moves, i.e., ρ_a, θ_a, and ϕ_a are assumed to be functions of time.

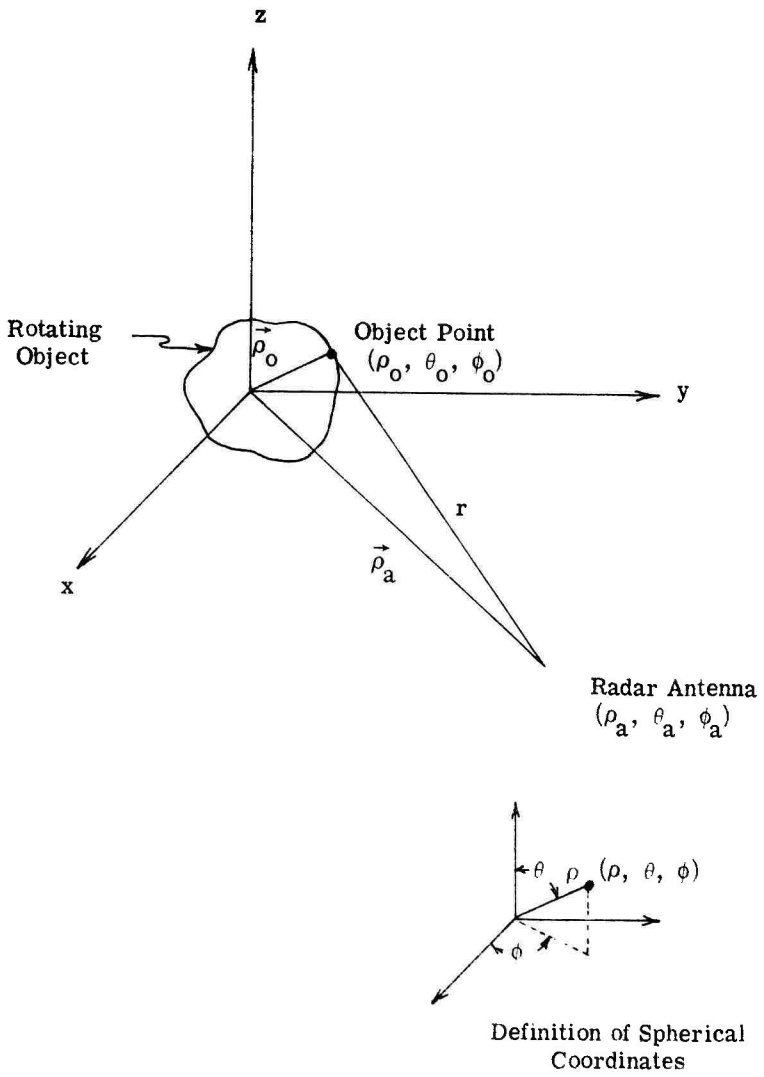

FIGURE 4. RADAR/OBJECT GEOMETRY

The radar transmits a sequence of linear FM pulses of the form

$$P_n(t) = A(t - nT) \exp j\left[2\pi f_c t + \frac{\gamma}{2}(t - nT)^2\right] \tag{13}$$

where A(t) is the amplitude weighting of each pulse, γ is the FM rate, $\frac{1}{T}$ is the PRF, and f_c is the center frequency.

The signal received from a scattering point at ρ_o, θ_o, ϕ_o is

$$\sigma_o A\left(t - nT - \frac{2r}{c}\right) \exp j\left[2\pi f_c\left(t - \frac{2r}{c}\right) + \frac{\gamma}{2}\left(t - nT - \frac{2r}{c}\right)^2\right] \tag{14}$$

where σ_o is the complex reflectivity of the point and includes two-way propagation effects and antenna gain.

In principle, the received signal can be demodulated by mixing it with a reference signal of the form

$$z(t) = \exp\left\{-j\left[2\pi f_c\left(t - \frac{2\rho_a}{c}\right) + \frac{\gamma}{2}\left(t - nT - \frac{2\rho_a}{c}\right)^2\right]\right\} \tag{15}$$

which also removes the effects of the time-varying range, $\rho_a(t)$, from the antenna to the rotating object. In practical radar receivers, several alternative techniques for removing gross range and Doppler effects are also possible.

The video signal resulting from the mixing operation can be expressed as

$$s(t, \hat{t}) = \sigma_o A\left[\hat{t} - \frac{2(r - \rho_a)}{c}\right] \exp\left[-j\left(\frac{4\pi}{\lambda} + \frac{2\gamma\hat{t}}{c}\right)(r - \rho_a) + j\left(\frac{2\gamma}{c^2}\right)(r - \rho_a)^2\right] \tag{16}$$

where $r - \rho_a = -\rho_o [\cos\theta_a \cos\theta_o + \sin\theta_a \sin\theta_o \cos(\phi_o - \phi_a)]$

$$\hat{t} = t - nT - \frac{2\rho_a}{c}$$

λ = radar wavelength

If the radar pulse length is long compared to $\frac{2(r - \rho_a)}{c}$, the video signal is approximately

$$s(t, \hat{t}) = \sigma_o A(\hat{t}) \exp\left\{\left(\frac{4\pi}{\gamma} + \frac{2\gamma\hat{t}}{c}\right)\rho_o [\cos\theta_a \cos\theta_o + \sin\theta_a \sin\theta_o \cos(\phi_o - \phi_a)]\right\} \tag{17}$$

For the special case of an object rotating at an angular rate Ω and the radar line-of-sight perpendicular to the axis of rotation, Eq. (17) can be greatly simplified. This is mathematically equivalent to setting $\theta_a = 90^o$, assuming a fixed object, and allowing the antenna to move around the object (i.e., $\phi_a = \Omega t$).

The video signal then becomes

$$s(t, \hat{t}) = \sigma_o A(\hat{t}) \exp\left[-j\left(\frac{4\pi}{\gamma} + \frac{2\gamma\hat{t}}{c}\right) r_o \cos(\phi_o - \Omega t)\right] \tag{18}$$

where $r_o = \rho_o \sin\theta_o = \sqrt{x_o^2 + y_o^2}$

Note that in this case all information about the vertical location z_o of the point scatterer has been lost. More general situations in which the radar line-of-sight is not perpendicular to the axis of rotation will be considered later in this section.

To enable optical processing of the radar data, the video signal, Eq. (18), is recorded on a suitable recording material (e.g., photographic film or thermoplastic) in a polar format as shown in Fig. 5. The recording format is chosen so that the spatial polar coordinates (r_F, ϕ_F) of the recorded signal are given by

$$r_F = v_s\left(\hat{t} + \frac{2\pi c}{\gamma\lambda}\right) \tag{19}$$

$$\phi_F = \Omega t \tag{20}$$

where v_s is the sweep velocity of the writing beam.

The relative values of the radial interval Δr and the mean radius r_m of the annular recording region shown in Fig. 5 are determined by Eq. (19). Since $-(T_p/2) < \hat{t} < (T_p/2)$ where T_p is the transmitted pulse length, the radial interval of the recording region is

$$\Delta r = v_s T_p$$

The mean radius is

$$r_m = \frac{2\pi c v_s}{\gamma\lambda}$$

Therefore,

$$\frac{\Delta r}{r_m} = \frac{T_p \gamma\lambda}{2\pi c} = \frac{\Delta f}{f_c} \tag{21}$$

where Δf is the bandwidth of the transmitted signal and f_c is the center frequency.

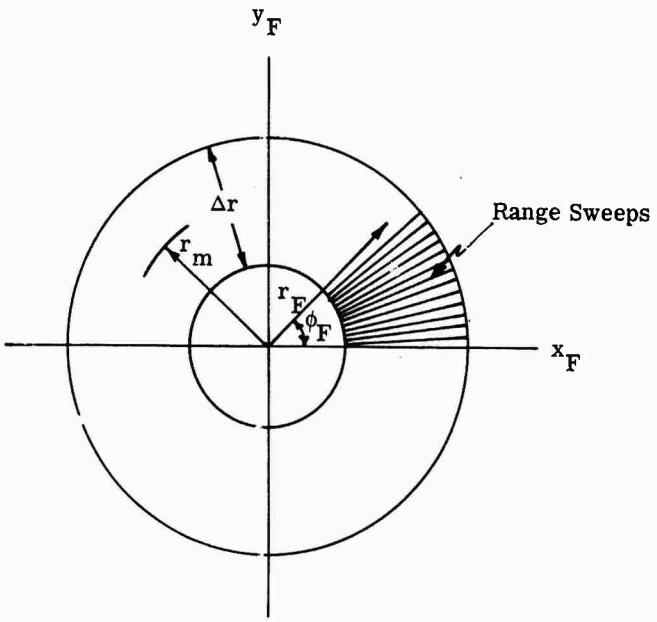

FIGURE 5. POLAR RECORDING FORMAT

After recording the video signal (Eq. 18) in a polar format, the resulting two-dimensional variation of light amplitude transmittance corresponding to a single point scatterer located at ρ_o, θ_o, ϕ_o is

$$s_p(r_F, \phi_F) = T_b + \tilde{A}(r_F)\sigma_o \cos\left[\frac{2\gamma}{cv_s} r_F r_o \cos(\phi_o - \phi_F)\right] \tag{22}$$

where T_b is the usual bias term required for recording the bipolar video signal and $\tilde{A}(r_F)$ represents an amplitude scaling factor which is zero outside the annular recording area shown in Fig. 5.

Expressed in terms of rectangular coordinates ($x_o = r_o \cos\phi_o$; $y_o = r_o \sin\phi_o$; $x_F = r_F \cos\phi_F$; $y_F = \sin\phi_F$), the recorded signal is

$$s_r(x_F, y_F) = T_b + B(x_F, y_F)\sigma_o \cos\left[\frac{2\gamma}{cv_s}(x_F x_o + y_F y_o)\right]$$

where

$$B(x_F, y_F) = \tilde{A}(r_F) \tag{23}$$

Equation (23) is an expression for a linear sinusoidal grating with x_F and y_F spatial frequency components proportional to x_o and y_o respectively. Therefore, a two-dimensional Fourier transform is the proper type of signal processing to produce an image of the point. Note that if instead of recording the video signal in a polar format as described by Eqs. (19) and (20), we had used the usual rectangular format such that

$$y_F = v_x \hat{t} \tag{24}$$

$$x_F = v_F t \tag{25}$$

where v_F is the translation velocity of the recording film, then we would not have obtained the simple linear grating type of recording given by Eq. (23). The spatial signal resulting from rectangular format recording consists of a family of curved lines as indicated in Fig. 2(a) of Section 2.

The total recorded signal for the entire object can be obtained by summing contributions from each element of the object. For the case under consideration here (radar line-of-sight perpendicular to rotation axis), the signal does not depend on the z_o coordinate of each scattering point and the recorded signal can be expressed as

$$s_p(r_F, \phi_F) = T_b + A(\tilde{r}_F)\iint \sigma(r_o, \phi_o) \cos\left[\frac{2\gamma}{cv_s} r_F r_o \cos(\phi_o - \phi_F)\right] r_o \, dr_o \, d\phi_o \qquad (26)$$

where $\sigma(r_o, \phi_o) r_o \, dr_o \, d\phi_o$ is the reflectivity associated with the differential element of volume shown in Fig. 6.

An image of the object is defined to be an estimate of the reflectivity density $\sigma(r_o, \phi_o)$ and can be obtained by optically carrying out a two-dimensional Fourier transform of $s_p(r_F, \phi_F)$. The image in this case appears as the projection of all scattering points of the three-dimensional object shown in Fig. 4 onto the x, y plane.

For the case of a three-dimensional rotating object where the radar line-of-sight is not perpendicular to the axis of rotation ($\theta_a \neq 90^o$, $\phi_a = \Omega t$), the appearance of the resulting imagery may be quite different. Instead of using Eq. (18) as a description of the video signal, we must consider the more general expression given by Eq. (17). In this case, one sideband of the recorded signal corresponding to a point scatterer located at ρ_o, θ_o, ϕ_o is of the form

$$s_p(r_F, \phi_F) = \sigma_o \tilde{A}(r_F) \exp j\left\{\frac{2\gamma}{cv_s} r_F \rho_o [\cos\theta_a \cos\theta_o + \sin\theta_a \sin\theta_o \cos(\phi_o - \phi_F)]\right\} \qquad (27)$$

This can be rewritten as

$$s_p(r_F, \phi_F) = \sigma_o \tilde{A}(r_F) \exp j\left(\frac{2\gamma}{cv_s} r_F z_o \cos\theta_a\right) \exp j[r_F \tilde{r}_o \cos(\phi_o - \phi_F)] \qquad (28)$$

where $\tilde{r}_o = r_o \sin\theta_a$ and indicates that the image size is scaled by $\sin\theta_a$. The factor $\exp j\left(\frac{2\gamma}{cv_s} r_F z_o \cos\theta_a\right)$ represents a rotationally symmetric phase error and the two-dimensional Fourier transform of $s_p(r_F, \phi_F)$ is approximately a ring distribution with a radius proportional to $z_o \cos\theta_a$.

For example, if we have a rotating object comprised of five point scatterers as shown in Fig. 7(a) and the radar antenna is located such that $\theta_a \neq 90^o$, the resulting image would be as shown in Fig. 7(b). When $\theta_a = 90^o$, the central ring image reduces to a point as shown in Fig. 7(c).

If we have a priori knowledge that the object is made up of only point scatterers then the location of the rings in the image and their radii could be measured to estimate the three-dimensional size and shape of the object. For actual objects there would be an ambiguity caused by an actual reflecting ring and a point scatterer located above or below it.

An image such as the one sketched in Fig. 7(b) is produced only if we process the radar signal over an interval corresponding to a full 360^o rotation of the object. By processing over

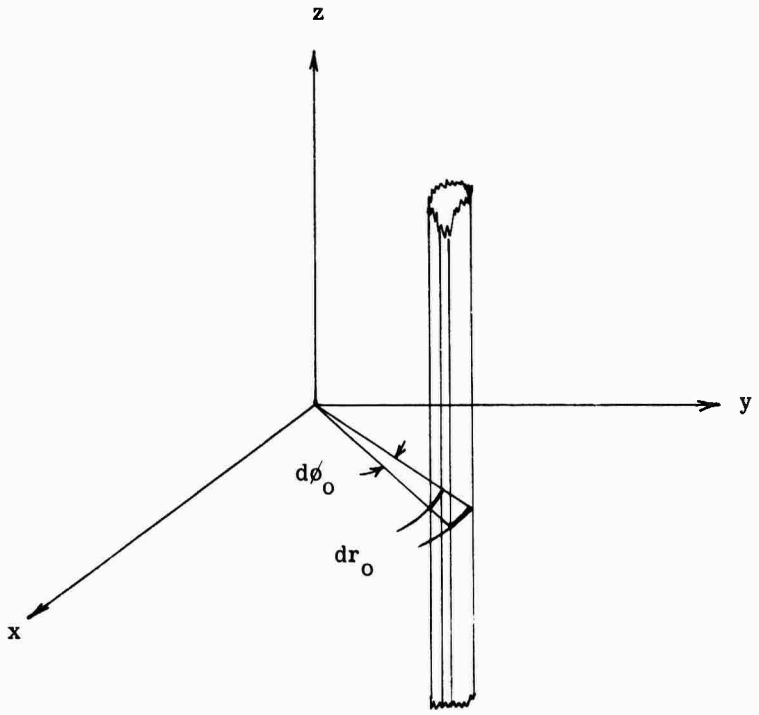

FIGURE 6. EFFECTIVE RESOLUTION CELL WHEN RADAR LINE OF SIGHT IS PERPENDICULAR TO ROTATION AXIS

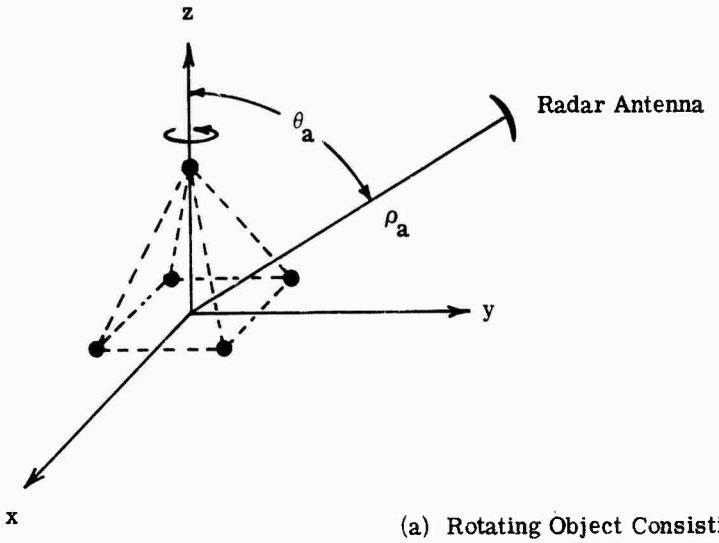

(a) Rotating Object Consisting of Five Point-Scatterers

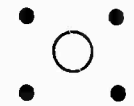

(b) Image for the Case When $0 < \theta_a < 90^o$

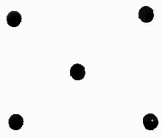

(c) Image for the Case When $\theta_a = 90^o$

FIGURE 7. DIAGRAM SHOWING ANTENNA ANGLE EFFECT IN IMAGES OF THREE-DIMENSIONAL ROTATING OBJECTS

smaller intervals or if the object point is visible only over part of the rotation, we would get arc-like images instead of rings for points located above or below the x, y reference plane of the object.

4
EXPERIMENTAL INVESTIGATION OF POLAR RECORDING FORMAT TECHNIQUE

This section describes the instrumentation and procedures employed to investigate optical processing of rotating-object radar data using a polar recording format. Examples of radar imagery from a variety of test objects placed on a rotating platform are presented.

4.1. ROTATING PLATFORM RADAR FACILITY

A simple diagram of the ERIM X-Band Rotating Platform Radar Facility used to simulate a satellite object imaging radar system in this investigation is shown in Fig. 8. This facility was constructed originally for target signature studies of various military vehicles [8]; however, simple modifications permitted its use in the work described herein.

Separate transmitting and receiving horns were used and located about 44 meters from the center of the platform. The platform is about 6 meters in diameter and has a rotation period of 168 seconds. Figure 9 is a photograph of the actual platform.

The more important radar parameters are given in Table 1. A highly simplified block diagram of the radar system is shown in Fig. 10. This system represents a form of a Stretch [11] radar and serves to greatly reduce the bandwidth of the video signal relative to the transmitted bandwidth. Long (up to 800 μS) chirp pulses with an FM rate of 4.5 MHz/μsec are transmitted. The received signal is mixed with a reference signal derived by appropriately delaying a portion of the transmitted chirp signal. A point scatterer on the rotating platform then produces constant-frequency pulses at the output of the mixer. The frequency of each pulse is proportional to the range of the point scatterer. With the proper length of coaxial delay line, the center of the platform can be made to correspond to a frequency of zero and the edge of the platform to about 90 kHz. Thus, even though the transmitted bandwidth is 3.6 GHz, the video bandwidth is about 90 kHz for the 6 meter diameter platform.

TABLE 1. ROTATING PLATFORM RADAR PARAMETERS

Transmitter center frequency	10.1 GHz
Maximum bandwidth	3.6 GHz
PRF	200 pulses/sec
Pulse width	800 μsec

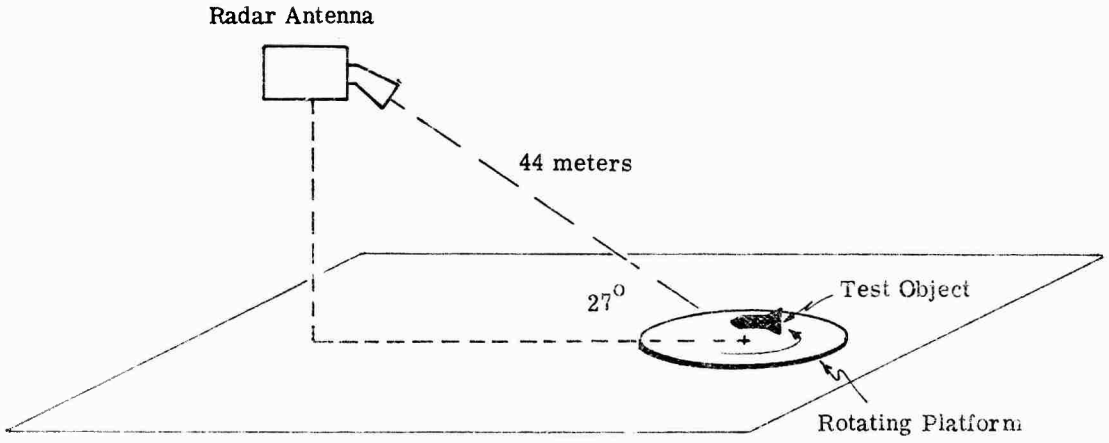

FIGURE 8. DIAGRAM OF ROTATING PLATFORM FACILITY USED TO SIMULATE A SATELLITE-OBJECT IMAGING RADAR

FIGURE 9. ROTATING PLATFORM RADAR FACILITY

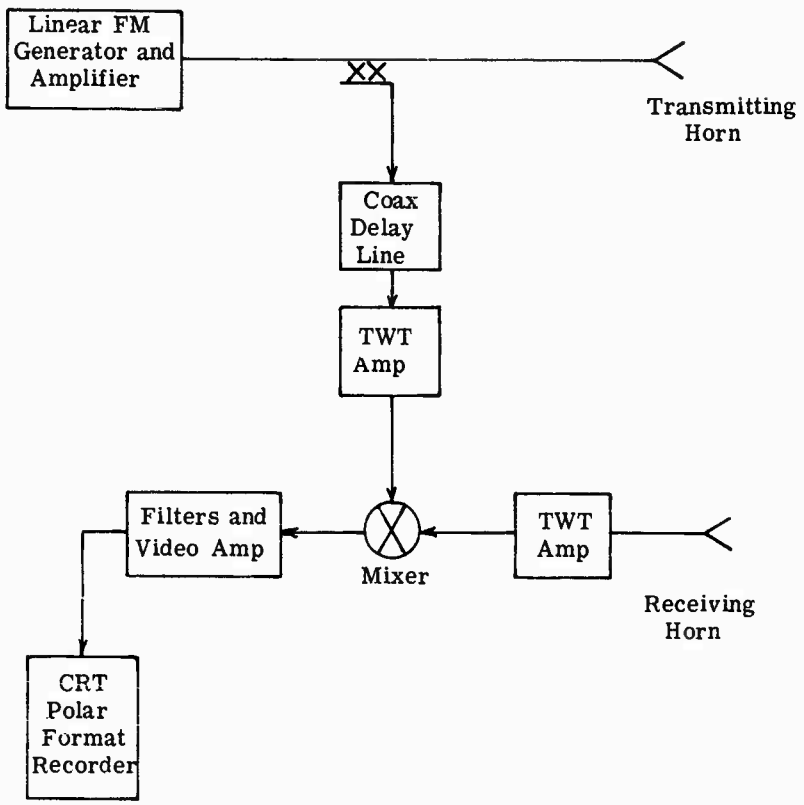

FIGURE 10. BLOCK DIAGRAM OF ROTATING PLATFORM RADAR SYSTEM

4.2. IMPLEMENTATION OF POLAR FORMAT RECORDING

Our earlier experimental work to verify the polar format concept relied primarily on recording the radar data on film in a rectangular format and then using an optical system to effect the rectangular-to-polar conversion. This was done by imaging a slit-type illumination source onto a rotating photographic plate. By then translating the rectangularly formated data across the slit source at the proper rate, the desired polar format recording could be produced on the photographic plate.

For the investigations conducted under the present contract, a new breadboard film recorder [see system schematic, Fig. 3(a)] was constructed to record the radar data directly in a polar format. A photograph of the actual breadboard recorder appears in Fig. 11. The recorder consists basically of a 70 mm roll-film holder attached to a motor-driven Troyke precision rotary table. The rotation rate of the recorder can be adjusted to match the rotation rate of the radar test targets. Positional adjustments are also provided for focusing and properly scaling the polar format recording. The line-scan CRT and other parts of the total recording system are standard components of the Rotating Platform Radar Facility described in Ref. [8].

After each recording (corresponding to one revolution of the object), the film can be advanced to a new frame so that a sequence of polar recordings for different objects or different radar parameters can be stored on a single filmstrip. Figure 12 shows a portion of a typical polar-format data film.

4.3. OPTICAL PROCESSING

As discussed previously, an image of a rotating object can be obtained by Fourier-transform processing the polar format recording. Since a spherical lens produces a two-dimensional Fourier-transform relationship between the complex amplitude of the light distribution in its front and back focal planes, the basic optical processor shown in Figs. 13 and 14 is readily implemented with few components.

In addition to the Fourier-transforming lens, other standard optical components are required to expand and collimate the laser beam. The image plane can either be examined by means of a microscope as indicated in Fig. 14 or a camera can be used to make a permanent film recording. Alternatively, a projection lens may be used to display the image on a viewing screen.

In Section 3 we observed that radar data for each point scatterer of a rotating object is recorded on the polar-format signal film as a two-dimensional diffraction grating of the form

$$s_r(x_F, y_F) = T_b + T_1 \cos K(x_o x_F + y_o y_F) \tag{29}$$

where $s_r(x_F, y_F)$ is the light amplitude transmittance of the film, T_b the average transmittance, T_1 the amplitude of the spatial modulation, and the constant $K = 2\gamma / cv_s$.

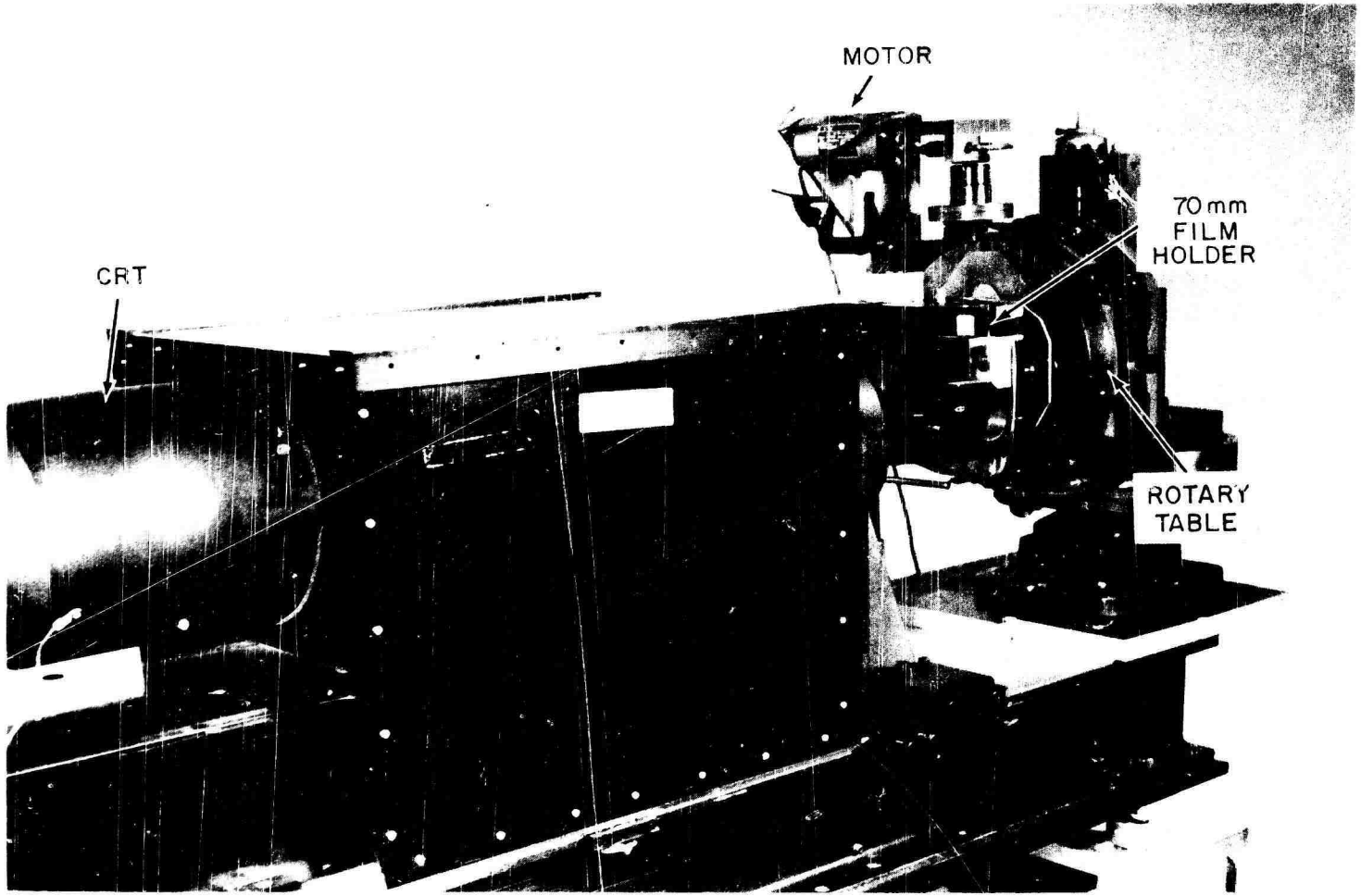

FIGURE 11. POLAR FORMAT FILM RECORDER

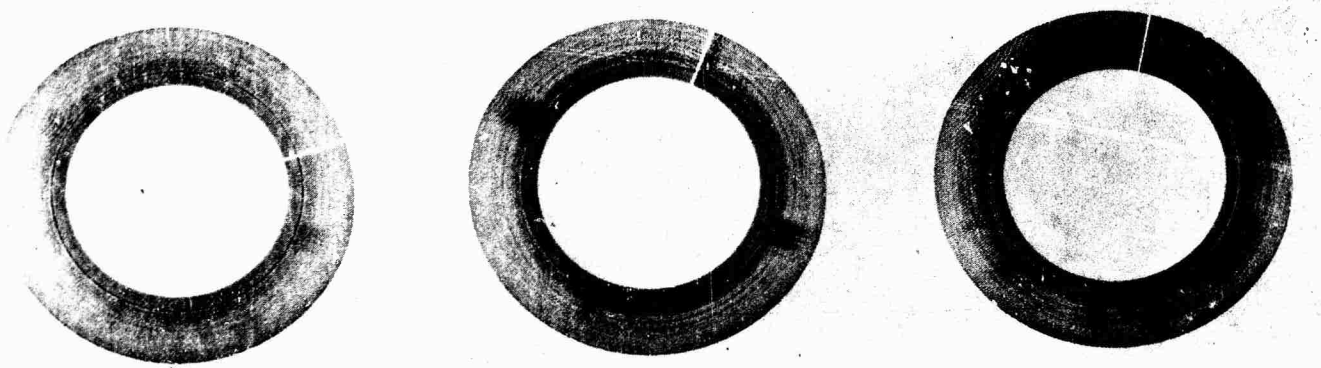

FIGURE 12. EXAMPLE OF POLAR FORMAT DATA FILM

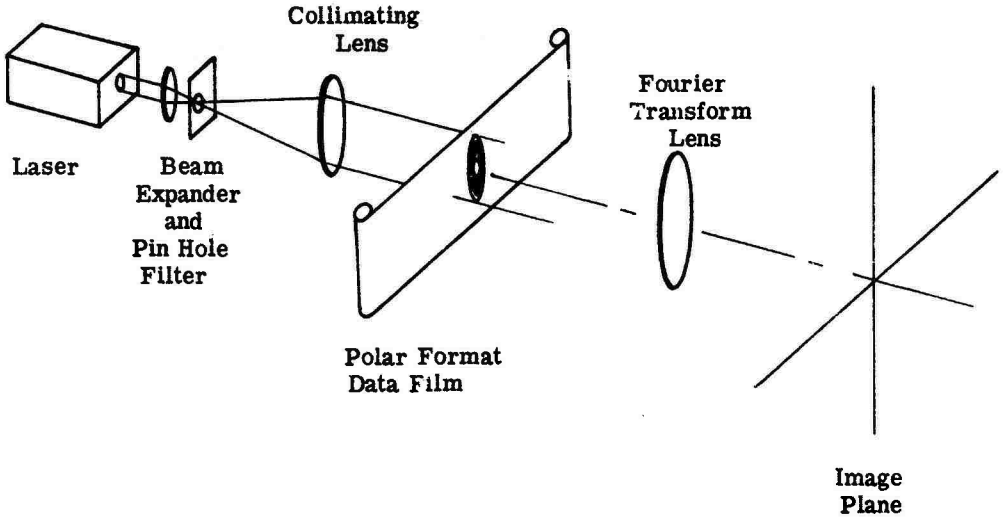

FIGURE 13. DIAGRAM OF OPTICAL PROCESSOR

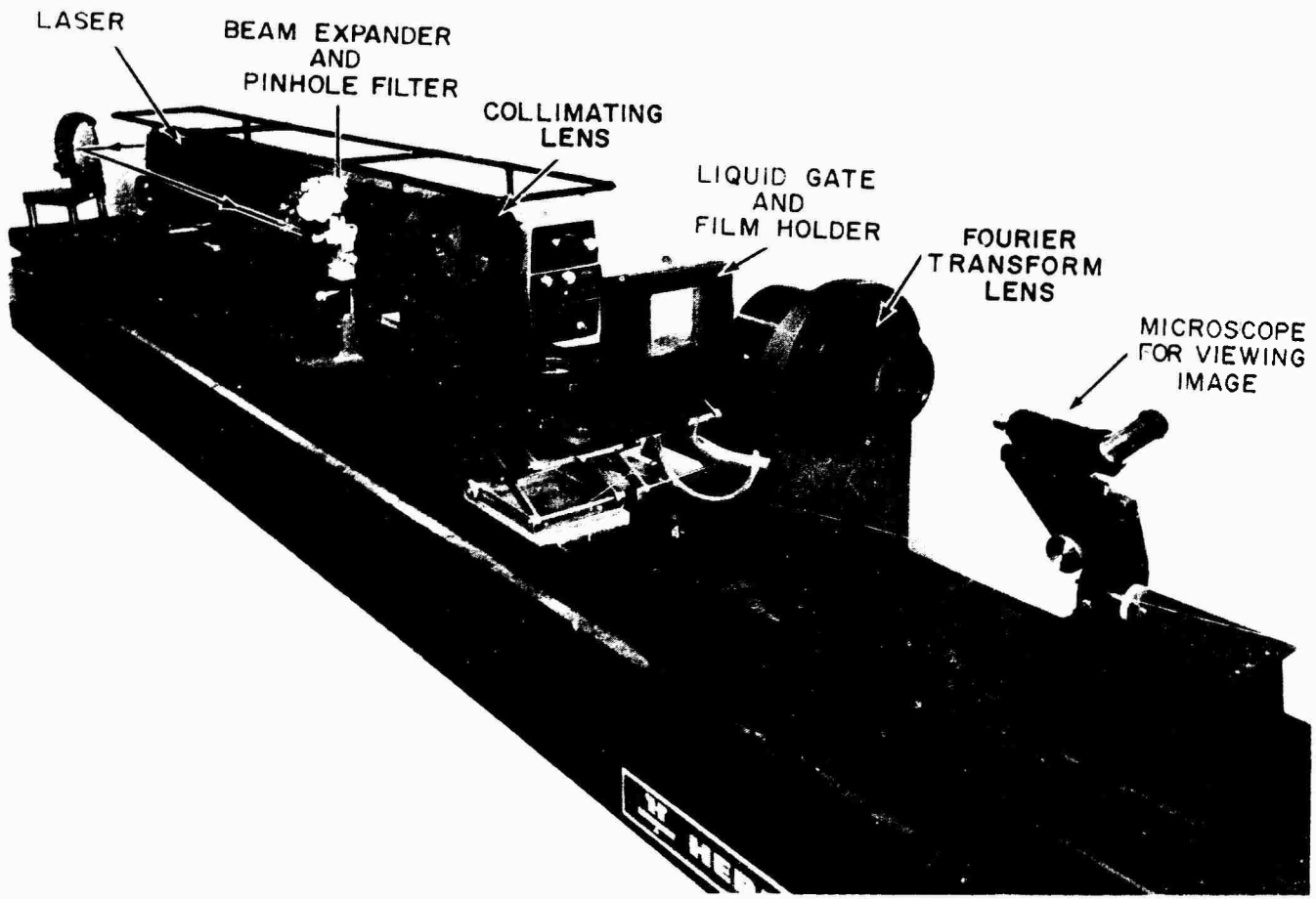

FIGURE 14. OPTICAL PROCESSOR

The Fourier transform of such a sinusoidal grating is made up of three terms often called the zero-order and the plus and minus first orders [9]. The zero-order spectrum is located on the optical axis at the center of the image plane whereas the two first-order spectra are symmetrically located at a distance from the center proportional to the spatial frequency of the grating—i.e., at a radius proportional to $x_o^2 + y_o^2$, the radial position of the point scatter from the center of rotation.

Therefore, each point scatterer of a rotating object produces a pair of conjugate point images. For example, an array of three corner-reflectors on the rotating platform as sketched in Fig. 15(a), results in the total radar image shown in Fig. 15(b). Since the corner reflectors were located away from the center of rotation and there were no targets on the opposite side of the platform, there is no ambiguity and a good image of the corner-reflector array can be obtained. If on the other hand the corner-reflectors are located around the center of rotation as shown in Fig. 16(a), we obtain an ambiguous image which is degraded further by the zero-order light [see part (b) of same figure].

For cooperative targets such as the rotating platform, the problem can of course be avoided by simply placing the object to be imaged away from the center of the platform. In practical space-object imaging problems, the two conjugate images should be separable even when the center of rotation lies within the object. This topic is discussed separately in Section 5.

By using apertures of various sizes and shapes at the input film plane, imagery with a variety of range and cross-range resolutions can be obtained. Since the radial interval of the polar format recording is proportional to the transmitted bandwidth, the fraction of the actual transmitted bandwidth used in the optical processor can be controlled by choosing the size of the radial interval of the processing aperture. Similarly, radar data can be processed over different angular intervals of object rotation by using an aperture that encompasses a corresponding angular interval of the polar format recording.

Normally, when processing radar data from a rotating object over small angular intervals of rotation $\Delta\phi$, range resolution (measured along radar line-of-sight) is inversely proportional to the transmitted signal bandwidth, whereas cross-range resolution varies inversely with $\Delta\phi$. However, for large $\Delta\phi$, resolution in both dimensions of the rotating object improves with increasing $\Delta\phi$.

For example, Fig. 17 shows a sequence of system impulse responses corresponding to three different processing apertures. The photographs were produced by magnifying the light distribution at the output of the optical processor (Fig 14) with the appropriate aperture at the input film plane. The radial interval is constant for all three cases and corresponds to a constant effective transmitted bandwidth. As can be seen, the 90^o interval case has improved resolution in both dimensions even though the effective transmitted bandwidth remained the same. This implies that good two-dimensional resolution of rotating objects consisting of scattering centers visible over large angles of rotation can be theoretically obtained even with rel-

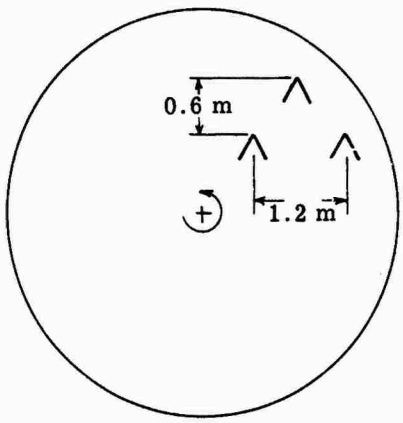

(a) Three Corner-Reflectors on Rotating Platform

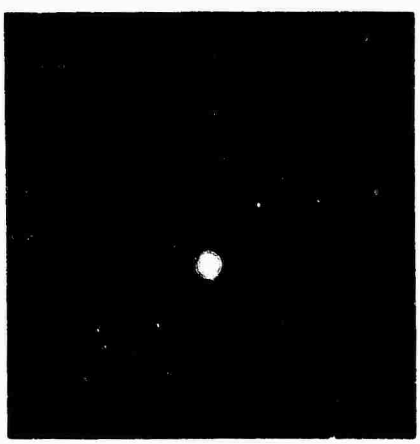

(b) Radar Image

FIGURE 15. EXAMPLE SHOWING SEPARATION OF CONJUGATE IMAGES

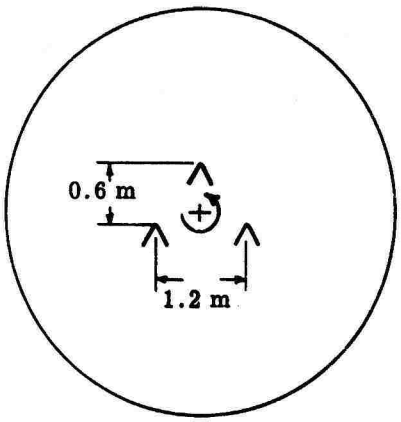

(a) Three Corner-Reflectors on Rotating Platform

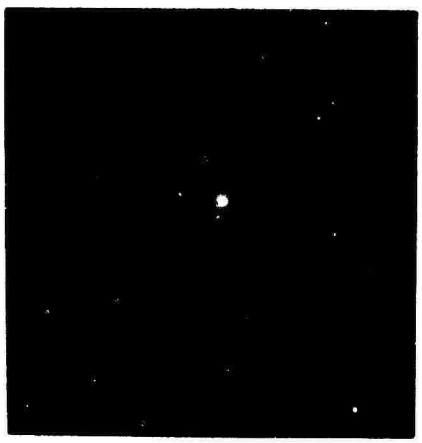

(b) Radar Image

FIGURE 16. EXAMPLE SHOWING CONJUGATE IMAGE AMBIGUITY

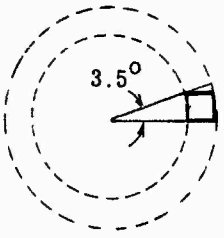

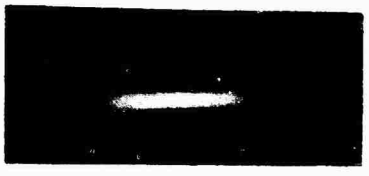

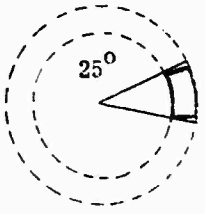

System Impulse Response

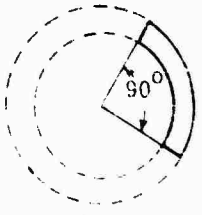

Processing Aperture

FIGURE 17. EFFECT OF PROCESSING APERTURE SHAPE ON SYSTEM IMPULSE RESPONSE

atively narrow bandwidth radars. The resulting impulse response sidelobe level may be intolerably large for some applications, however.

The ability to determine the size and shape of a specular object is greatly enhanced by processing the recorded data over large angular intervals. The resulting image then contains reflectivity information about the object over a wide range of aspect angles.

One way to perform such processing is to simply illuminate the full 360° of the polar format recording in the optical processor. Instead of coherently processing over the full annulus, one can also use a coherent processing aperture of a size sufficient to produce the desired resolution and then move the aperture around the entire 360° of the recording while continually exposing a piece of film at the image plane. The resulting image consists of a noncoherent summation of an infinite number of coherently processed images. This is often called "mixed" processing. Various experimental examples of imagery produced by coherent and mixed processing are presented in the next section.

4.4. EXPERIMENTAL RESULTS

A number of rotating-object imaging experiments were performed with the instrumentation described previously. Some examples of imagery are given in this section to compare the rectangular- and polar-format approaches and to demonstrate the fine resolution and object shape recognition capability afforded through use of a polar recording format. In these experiments horizontal polarization was used for both transmitting and receiving.

(C) To demonstrate the improved resolution obtainable by using a polar recording format instead of the usual rectangular format, an experiment was performed in which three corner-reflectors were placed on the rotating platform. Radar data for this corner array were recorded in both a rectangular and polar format. The resulting optically processed imagery is shown in Fig. 18. The spacing of the corner-reflectors was 1 ft. To produce parts (a) and (d) of this figure, we used a very small, square, processing aperture so that the three corner-reflectors are not resolved in either the rectangular or polar case. Results, shown in part (b) and (e) of the same figure, were obtained by using a square processing aperture of a size sufficient to barely resolve the three corners. If the processing aperture size is increased, we see that for the rectangular case (c) the phase errors resulting from motion through resolution cells produce a very degraded image, whereas in the polar case (f) improved resolution is achieved.

(C) Figure 19 presents a further example of the image degradation caused by the problem of motion through resolution cells inherent in rectangular format processing. This result was obtained by rectangular format processing of radar returns from a 31 cm diameter cylinder placed on the rotating platform as indicated in the photograph [Fig. 19(a)]. This sequence of images again shows the smearing produced by processing rectangular format data over large angles of rotation. As a reference, part of the zero order diffraction pattern was retained in parts (b), (c), (d) of the same figure; it denotes the center of rotation which was about 1.5 meters from the cylinder. For comparison, radar data from the same cylindrical object were re-

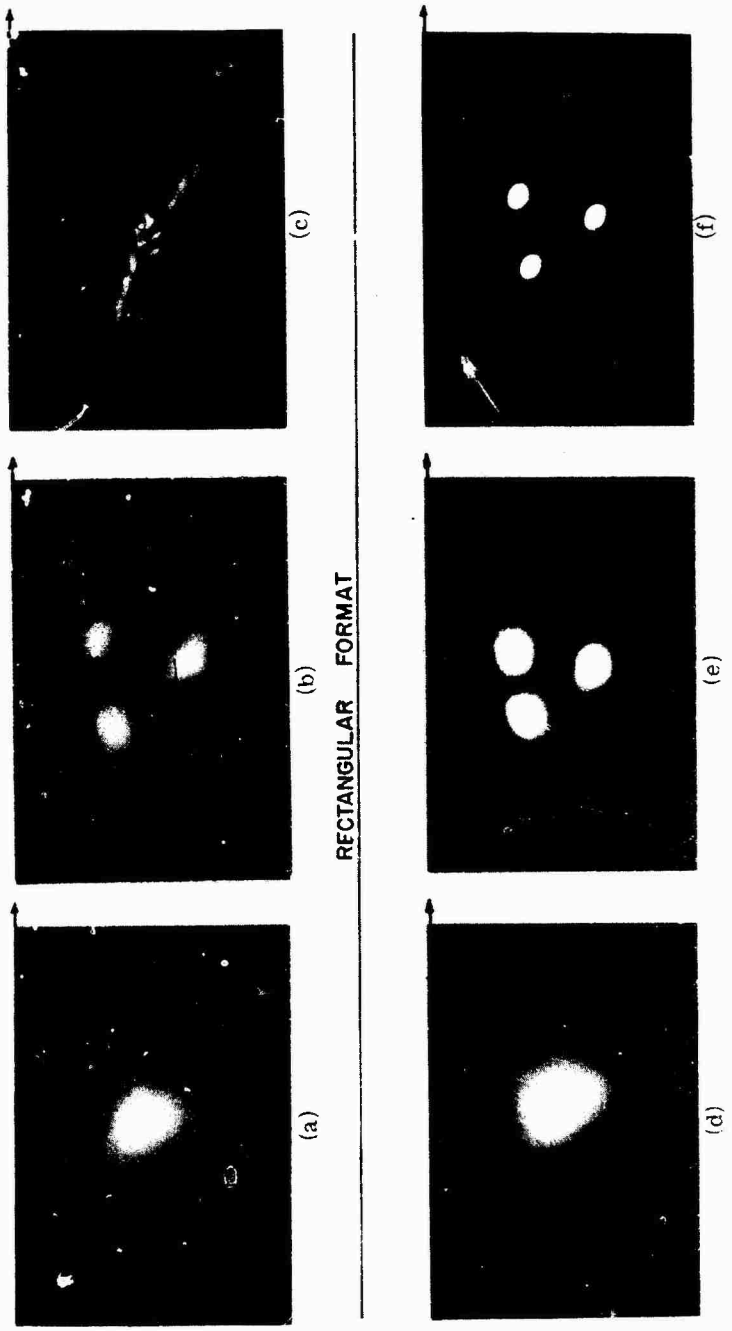

FIGURE 18. COMPARISON OF RECTANGULAR AND POLAR FORMAT PROCESSING FOR THREE CORNER REFLECTORS

(a) Photograph of Cylinder on Rotating Platform

(b) Δf = 1.1 GHz
$\Delta\phi = 6^{o}$

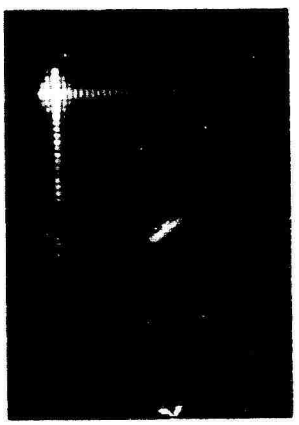

(c) Δf = 2.2 GHz
$\Delta\phi = 12^{o}$

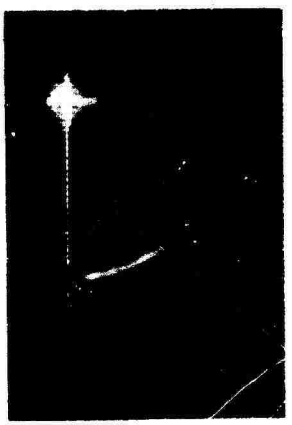

(d) Δf = 2.2 GHz
$\Delta\phi = 35^{o}$

FIGURE 19. IMAGERY OF CYLINDRICAL TEST OBJECT SHOWING EFFECTS OF MOTION THROUGH RESOLUTION CELLS (EFFECTIVE TRANSMITTED BANDWIDTH Δf, PROCESSING ANGLE $\Delta\phi$)

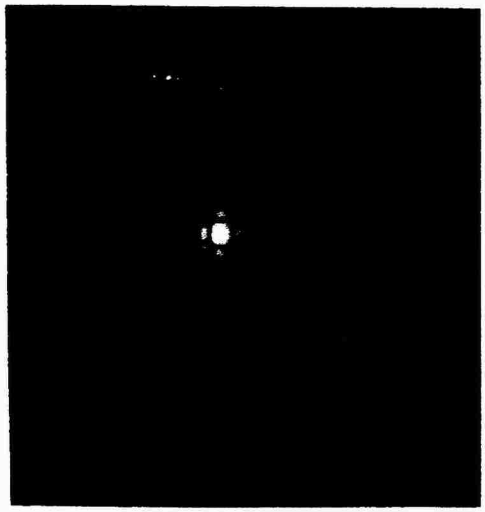

(a) Δf = 1.1 GHz
$\Delta\phi = 6^{o}$

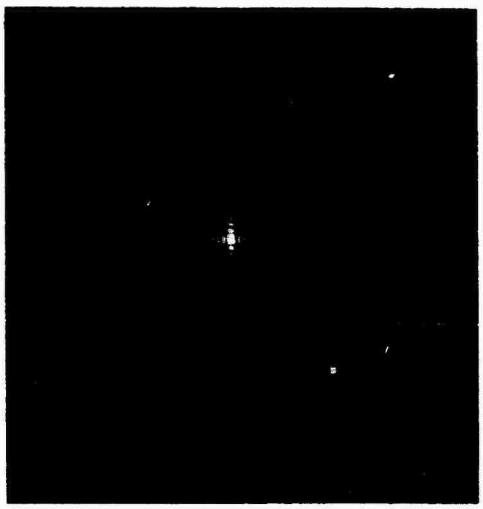

(b) Δf = 2.2 GHz
$\Delta\phi = 12^{o}$

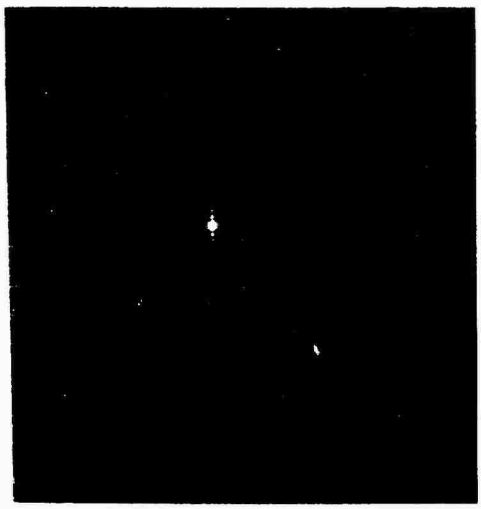

(c) Δf = 2.2 GHz
$\Delta\phi = 35^{o}$

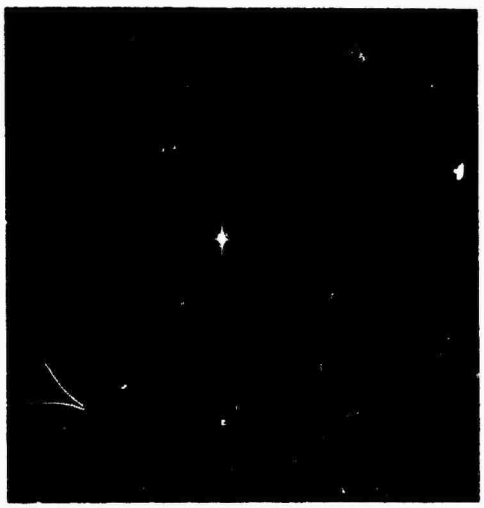

(d) Δf = 2.2 GHz
$\Delta\phi = 90^{o}$

FIGURE 20. IMAGERY OF CYLINDER PRODUCED BY POLAR FORMAT PROCESSING

corded in a polar format; the imagery produced by processing this data is shown in Fig. 20. The processing aperture sizes used to produce parts (a),(b),and (c) of Fig. 20 were the same as those used to produce the images in Fig. 19. The important point to note in comparing these two figures is that as the angular processing interval increases, not only do we obtain improved resolution but we can also begin to observe the circular shape of the object for the polar format case. (Recall that this radar imagery is similar to the view an observer would get by looking down on the rotating platform along its axis of rotation.) In the rectangular format case (Fig. 19), the smearing effect obscures the actual shape of the small object.

In Fig. 21 we have an example of the very fine two-dimensional resolution that can be achieved by using the polar recording format technique. In this experiment an array of small corner-reflectors was used as a test object on the rotating platform. The relative spacing of the corners is indicated in Fig. 21(a). The full 3.6 GHz transmitted bandwidth of the radar was used and the coherent angular processing interval was about 30^{o}. This is a resolution of nearly one wavelength and represents excellent performance for any type of imaging system.

(C) Examples of imagery in Figs. 22 through 26 illustrate the shape detectability which can be achieved by processing over a large change in aspect angle. The object shown in Fig. 22(a) consists of four 5-ft long pieces of 1-in. diameter pipe arranged on the rotating platform in the shape of an "M." By processing the radar data from this test object over a 90^{o} interval, the image in Fig. 22(b) was obtained.

(C) The object in Fig. 23(a) is a small aluminum cone-sphere. When radar returns from this object were coherently processed over a full rotation, a complete outline of the object was obtained as can be seen in Fig. 23(b). By using the mixed processing approach described previously, the image in Fig. 23(c) was obtained. A circular coherent processing aperture was used to produce a theoretical resolution of 9 cm in both range and cross-range. With incoherent summation carried out over the full 360^{o} of the recording, the shape of the entire object can again be seen. For simple specular objects such as this, mixed processing is often advantageous since it may produce a somewhat smoother image. It is necessary only to use a coherent processing aperture of a size to produce resolution fine enough to distinguish important object details. Much of the arc-like background noise that can be seen in the imagery is caused by radar returns from various stationary scatterers near the rotating platform. In rectangular format processing, stationary point-scatterers within the radar's field of view are imaged at their proper range and along the vertical axis (zero-Doppler line) of the image plane. This can be seen in much of the imagery presented in Ref. [6]. On the other hand, the polar format approach is designed to produce good images of rotating objects and, therefore, the images of stationary objects are dispersed and appear as background noise. Fortunately, this stationary clutter problem is of no concern for actual satellite imaging applications.

(C) Figure 24 further illustrates shape detectability. Here the test object consisted of two metal cylinders placed on the rotating platform as diagrammed in Fig. 24(a). Coherent processing over a small circular aperture to produce a two-dimensional resolution of 9 cm re-

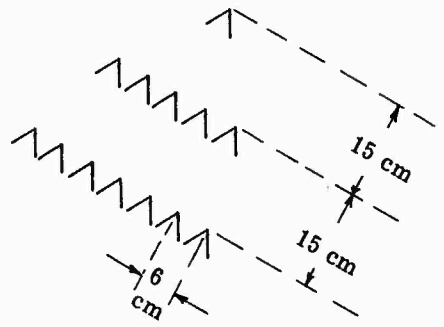

(a) Corner-Reflector Array

(b) Radar Image

FIGURE 21. EXAMPLE OF IMAGERY DEMONSTRATING VERY FINE RESOLUTION

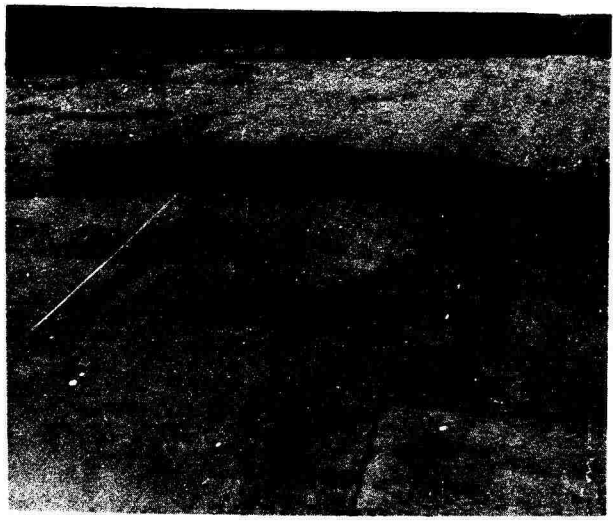

(a) Optical Image

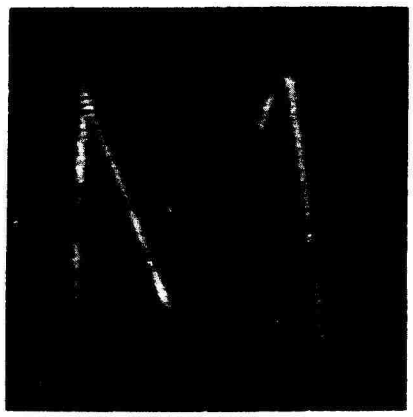

(b) Radar Image

FIGURE 22. IMAGE OF "M" TEST OBJECT

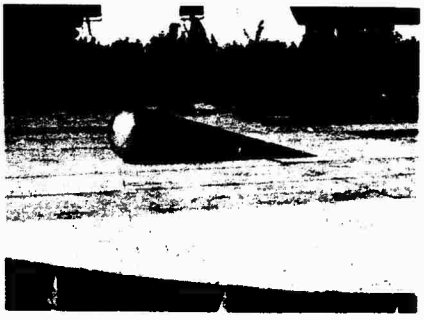

(a) Optical Image

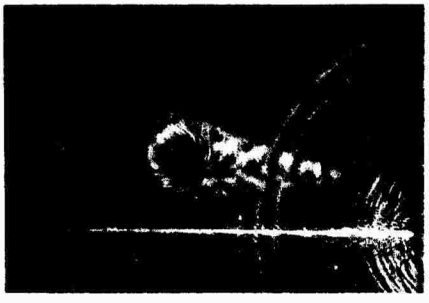

(b) 360^{O} Coherent Processing

(c) 360^{O} Mixed Processing

FIGURE 23. IMAGES OF CONE-SPHERE

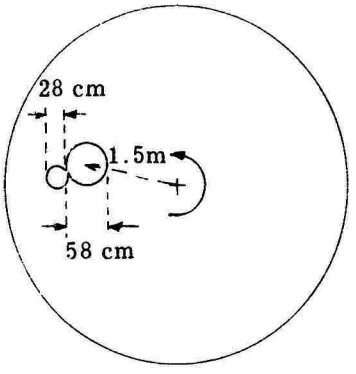

(a) Diagram Showing Location of Two Cylinders on Rotating Platform

(b) 10^{O} Coherent Processing Interval

(c) 180^{O} Mixed Processing

(d) 180^{O} Coherent Processing Interval

FIGURE 24. RADAR IMAGES OF TWO CYLINDERS

(a) Optical Image (b) Radar Image

FIGURE 25. IMAGE OF SIMULATED SPACE OBJECT

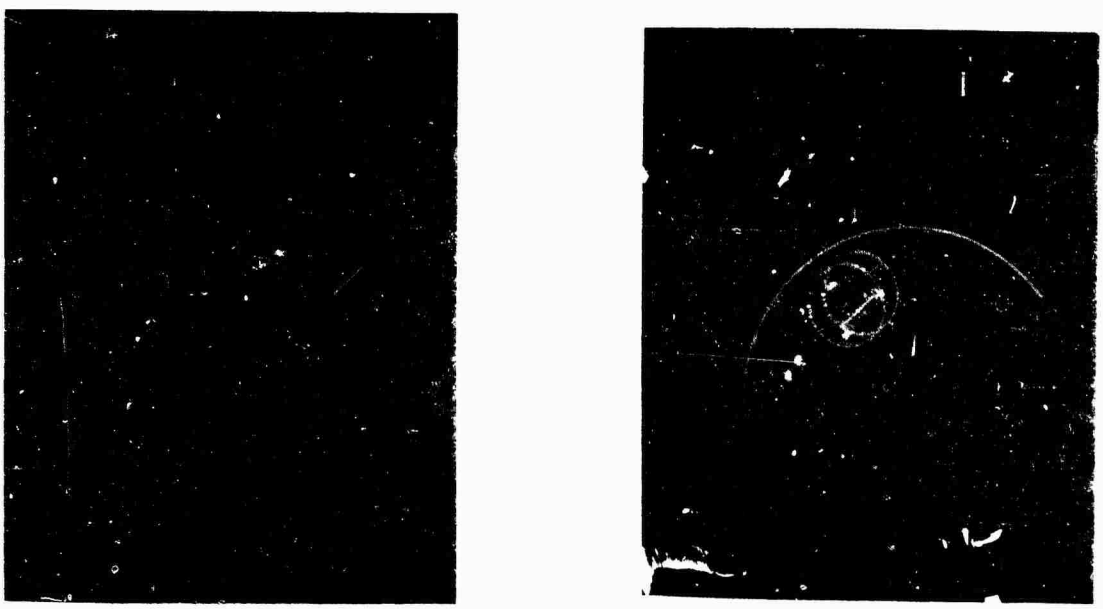

(a) 90^{O} Processing (b) 360^{O} Processing

FIGURE 26. RADAR IMAGES OF FOUR REFLECTORS — TWO ON PLATFORM SURFACE AND TWO 5 ft ABOVE SURFACE

sulted in the Fig. 24(b) image. Since the angular processing interval was only about 10^{o}, little shape information is obtained. Figures 24(c) and 24(d) show the results obtained by mixed and coherent processing over about 180^{o}. Again, if sufficient resolution is available, there is little difference between the mixed and coherently processed imagery in terms of shape detectability. The important point is that the processing be carried out over a large angular interval of object rotation.

Figure 25 shows the radar image obtained for a simulated space object (cone-cylinder-flare). Mixed processing was used over a full resolution and the shape of the object can be easily seen. Multiple-image effects are present because the surface of the rotating platform acts as a reflecting ground plane. Therefore, we get returns not only directly from the object itself but also from the object via the platform surface. By using crossed 45^{o} receiving and transmitting antenna polarization, it should be possible to suppress some of these multiple-bounce returns; however, polarization effects were not investigated during this program. The reflecting ground plane effects observed here are, of course, not important for space-object applications and, like the stationary clutter problem discussed previously, amounts only to an experimental inconvenience.

(C) The test object in this case is a Volkswagen. An image obtained by optically processing the radar data over 360^{o} of rotation is shown in Fig. A-1. Because of the fine resolution and the fact that the radar image contains relative reflectivity information over such a large change in aspect angle, many details of the VW can be observed in the image such as the fenders, bumpers, and indications of the seats.

(U) An interesting anomoly is that the right-hand door of the VW appears in the image as a line in the center instead of in the expected location. This can be explained with the aid of the diagram in Fig. A-2. In this experiment, the VW was located at the edge of the platform to avoid conjugate image ambiguities. Since the radar returns from vertical surfaces are primarily due to dihedral reflections and the platform surface is about 0.75 m above the ground, the effective range to the right door is significantly larger than the effective range to the other surfaces of the VW. This results in the observed displacement along the radar line of sight.

In Section 3 it was shown that for the case of a rotating object made up of a rigid three-dimensional collection of point-scatterers, the image consists of a family of overlapping circles when the radar line-of-sight is not perpendicular to the rotation axis and a 360^{o} angular processing interval is used. The system may be focused so that object points in any plane perpendicular to the rotation axis appear as point-like images. The image of any other object point is then still a circle with a radius proportional to the distance of the point away from the focused plane.

(C) This effect is not readily apparent in the previous images of relatively simple, specular objects. Accordingly, some experiments designed specifically to demonstrate the image effects for three-dimensional arrays of scatterers were performed. For example, Fig. 26 shows the results obtained for two small omni-directional reflectors located on the platform surface and two similar reflectors located 5 ft above the surface. The spacing between each pair of reflectors was 1 ft. The ring images (or 90^{o} arcs) correspond to the elevated reflectors, while the point-like images correspond to the reflectors on the surface. By adjusting the carrier frequency of the video signal, one can "focus" on the elevated points instead of on the platform surface. If this were done, the circles (or arcs) and the point-like images shown in Fig. 26 would be interchanged.

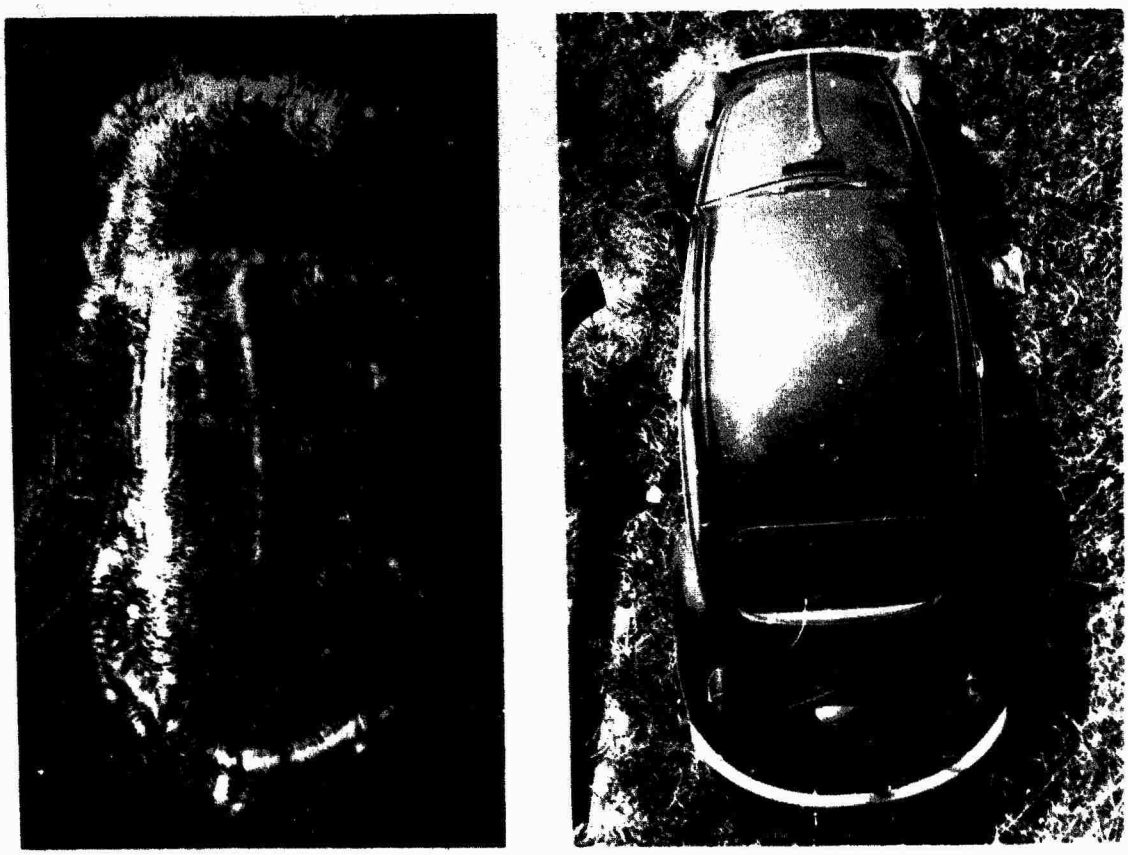

Confidential

FIGURE A-1. ROTATING PLATFORM RADAR IMAGE AND OPTICAL IMAGE OF A VOLKSWAGEN (U)

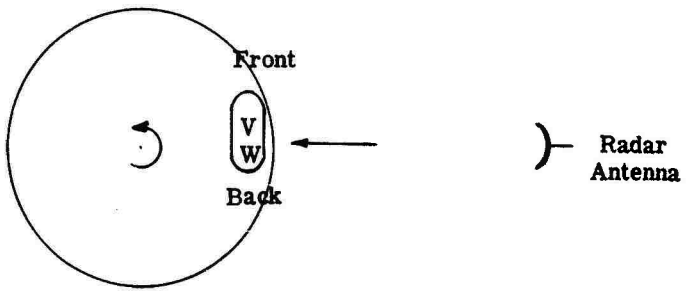

Top View of VW on Platform

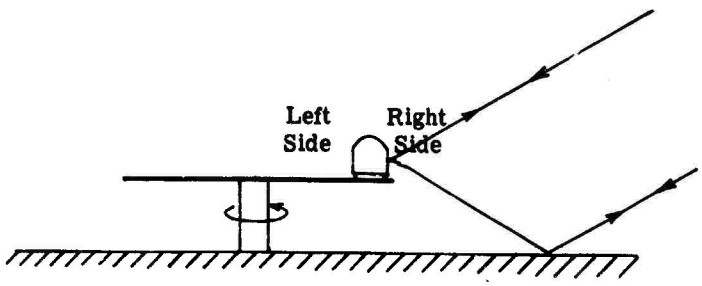

Side View of Platform - Position 1

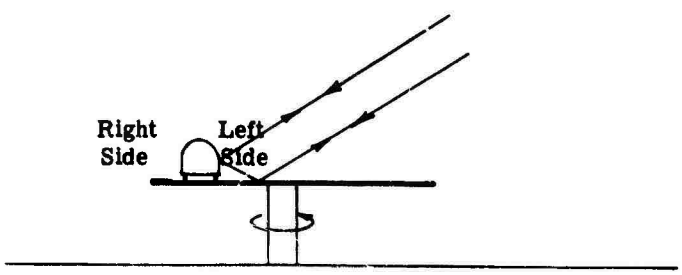

Side View of Platform - Position 2 Unclassified

FIGURE A-2. DIAGRAM ILLUSTRATING DIHEDRAL REFLECTIONS FOR RIGHT SIDE AND LEFT SIDE OF VW (U)

5
ELIMINATION OF CONJUGATE IMAGE AMBIGUITY

In practical rotating-object imaging systems, it is necessary to be able to separate the two conjugate images that appear at the output of the optical processor even when the center of rotation lies within the object. Usually in coherent optical data processing systems, this is done by causing the recorded signal to be on a spatial frequency offset carrier [10].

It was assumed for the discussion in Section 4 that the bandwidth of the video signal to be recorded was determined by the range extent of the object and that the video signal had zero carrier frequency. For rectangular-format recording systems, the desired spatial frequency offset can be easily achieved by allowing the video signal to have a carrier-frequency, i.e., a range-frequency offset. The carrier frequency component of the video signal at the input to the recorder results in a linear grating type of signal on the film; the returns from each point of the rotating object can thus be interpreted as amplitude and phase modulations of this spatial carrier. A Fourier transformation produces two conjugate images (within the usual rectangular format limitations) separated from each other in range by a distance proportional to the carrier frequency.

Instead of using a range-frequency offset, it is also possible to use cross-range or Doppler offset by introducing the proper pulse-to-pulse phase shift modulation in the receiver. In this case the two conjugate images are separated from each other in the cross-range dimension. Often a combination of range and cross-range offset is used for rectangular recording format systems.

The use of a polar recording format necessitates a modification of the usual frequency-offset approaches. Three of the techniques we investigated are presented below.

5.1. CONSTANT RANGE-FREQUENCY OFFSET

In a polar format recording, the video pulses are recorded along radial lines and, therefore, a carrier frequency component (range-frequency offset) appears on the recording material as a circular grating. This is shown in Fig. 27 in which an unrealistically low spatial frequency is used for illustrative purposes. Even though this type of spatial carrier allows the two conjugate terms of the recorded signal to be separated, it also introduces a rotationally symmetric phase error: for this reason a simple Fourier transform processor produces smeared imagery. To obtain high quality imagery, it is necessary to compensate for this phase error in the optical processor.

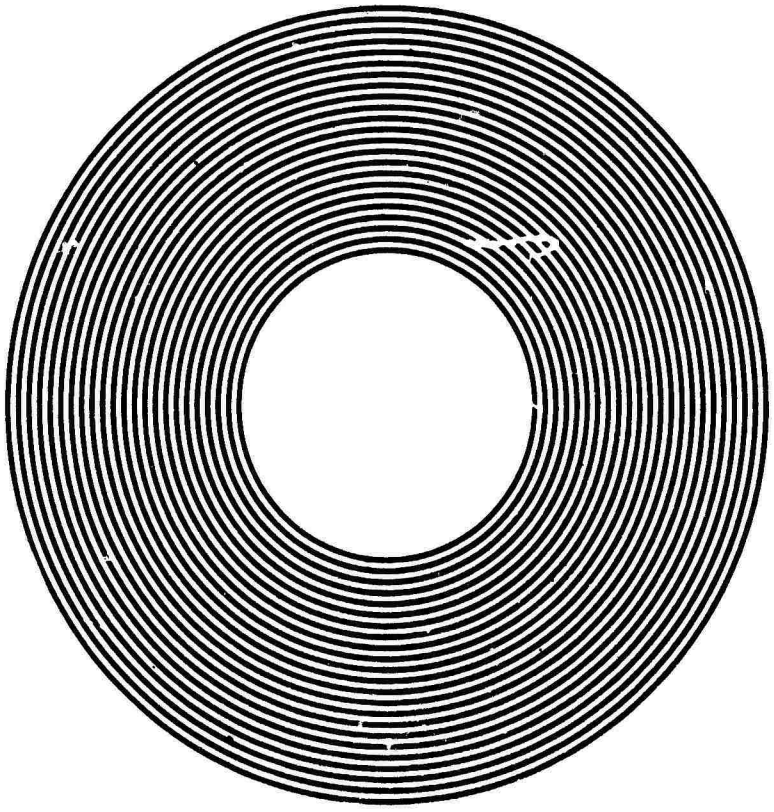

FIGURE 27. CONSTANT RANGE-FREQUENCY OFFSET SIGNAL RECORDED IN A POLAR FORMAT

The type of compensation required can be derived by modifying the expression for the video signal (Eq. 18) by introducing a carrier frequency (f_o) term. After being recorded in a polar format, the total signal for an object described by a reflectivity density $\sigma(r_o, \phi_o)$ is

$$s_p(r_F, \phi_F) = T_b + \iint \tilde{A}(r_F)\sigma(r_o, \phi_o) \cos\left[\frac{2\gamma}{cv_s} r_F r_o \cos(\phi_o - \phi_F) + \psi_1\right] \rho_o \, d\rho_o \, d\phi_o \qquad (30)$$

where

$$\psi_1 = \frac{2\pi f_o r_F}{v_s}$$

Note that this is the same as Eq. (26) except for the presence of the phase factor ψ_1.

Equation (30) can be rewritten as

$$s_p(r_F, \phi_F) = T_b + G \exp(j\psi_1) + G^* \exp(-j\psi_1) \qquad (31)$$

where

$$G = \frac{1}{2}\iint \sigma(r_o, \phi_o) \exp -j\left[\frac{2\gamma}{cv_s} r_F \rho_o \cos(\phi_F - \phi_o)\right] \rho_o \, d\rho_o \, d\phi_o \qquad (32)$$

i.e., G is the Fourier transform of the object reflectivity density $\sigma(r_o, \phi_o)$.

The degrading effects of the phase factor ψ_1 can be corrected by using the optical processing system shown in Fig. 28. At plane P1, lens 1 produces the two-dimensional Fourier transform of the recorded signal $s_p(r_F, \phi_F)$ and by means of a half-plane stop we can remove the zero order term and one sideband. That is, the only term which is allowed to pass is the Fourier transform of $G \exp j\psi_1$. A subsequent Fourier transform by means of lens 2 then produces a complex light amplitude distribution at plane P2 which is proportional to $G \exp j\psi_1$. A spatial filter with an amplitude transmittance of the form $\frac{1}{2}(1 + \cos\psi_1)$ is positioned at plane P2. The complex amplitude of the light emerging from P2 is

$$(G \exp j\psi)\left[\frac{1}{2}(1 + \cos\psi)\right] = \frac{G \exp j2\psi_1}{4} + \frac{G \exp j\psi_1}{2} + \frac{G}{4} \qquad (33)$$

Therefore, by taking a Fourier transform with lens 3, we get three spatially separated light distributions at the back focal plane of lens 3—one of which corresponds to the third term of the right-hand side of Eq. (33) and is the desired image of the rotating object. The other two are smeared versions of the image and can be blocked out.

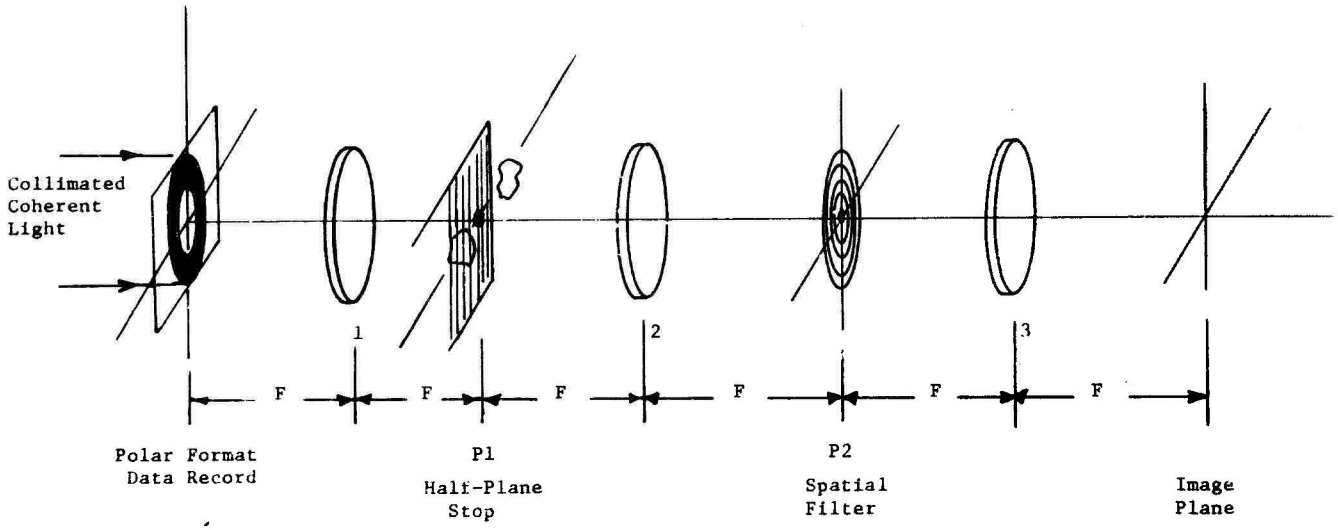

FIGURE 28. DIAGRAM OF OPTICAL SYSTEM FOR PROCESSING RANGE-FREQUENCY OFFSET DATA

Since the two-dimensional Fourier transform of exp $j\psi_1$ is approximately a ring distribution of light, we are restricted to coherently processing 180^0 or less of the input signal in order to separate the conjugate images adequately. By using mixed processing techniques, imagery containing information associated with all aspect angles can still be produced.

Some experiments were performed during this program to demonstrate the practical feasibility of using range-frequency offset with a polar recording format. Corner-reflector arrays and simple specular objects placed on the rotating platform were used in these experiments. A photograph of the actual optical processing system used is shown in Fig. 29.

The spatial filter was produced by sinusoidally intensity modulating a line-scan CRT and imaging the modulated line onto a piece of rotating film. The resulting record was then contact printed on a microflat photographic plate and optically bleached to produce the final spatial filter used in the system shown in Fig. 29

Figure 30 shows an experimental result for the case of three corner reflectors located at the center of the rotating platform. A range offset frequency (video carrier frequency) of 156 kHz was used. Recall that for the case of no frequency offset and Fourier transform processing, the degraded image shown in Fig. 16(b) was obtained. A contribution from each of the three terms indicated in Eq. (33) can be seen in Fig. 30. The set of three points at the right is the corrected image. The three arc-like images at the center, representing the image that would be obtained if no phase error compensation had been used, correspond to the second term in the right-hand side of Eq. (33).

Another example showing the use of a range-frequency offset and a polar recording format is given in Fig. 31. The object is an "M" constructed from four pieces of pipe as described in Section 3. In this case, however, the "M" was placed on the center of the rotating platform which necessitated the use of a frequency offset. Again, the corrected image can be seen along with the two uncorrected versions at the left. Since each of the elements of the object has a relatively narrow scattering angle, the primary effect in the uncorrected image is a displacement of the elements from their proper location.

5.2. LINEAR FM RANGE OFFSET

Another technique divised for eliminating the effects of the conjugate image has some advantages over the constant range-frequency offset approach. This technique also requires a nonzero video carrier frequency; however, a small amount of linear frequency-modulation is also added to each pulse. This addition can be implemented quite easily in the radar receiver by mixing the collection of linear FM signals returned from the target with a reference linear FM signal having a different chirp rate. When these video chirp pulses are recorded in polar format, the signal associated with the center of rotation of the target becomes an annular section of a Fresnel zone plate as shown in Fig. 32.

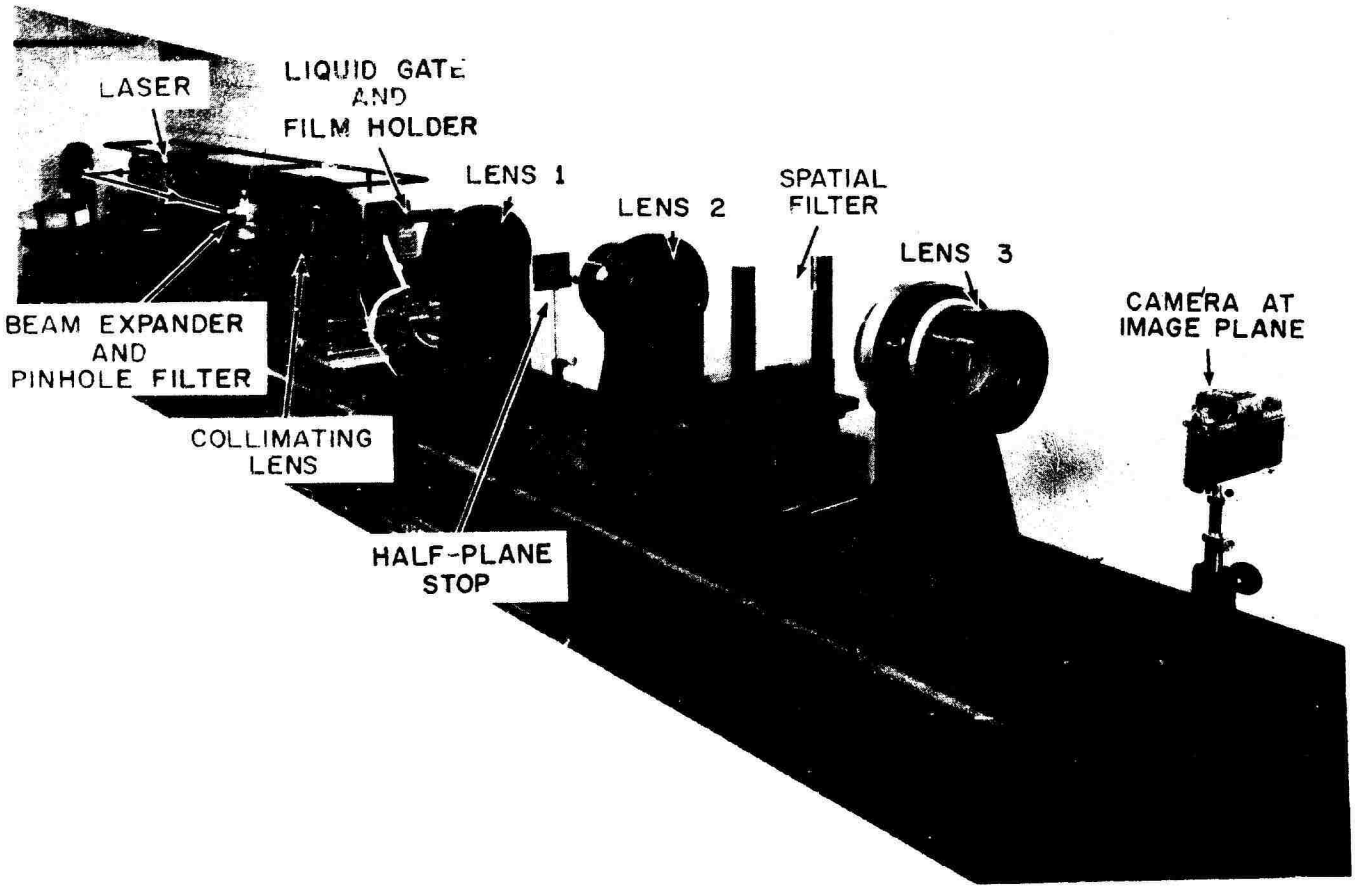

FIGURE 29. OPTICAL PROCESSOR FOR RANGE-FREQUENCY OFFSET DATA

FIGURE 30. IMAGE OF THREE CORNER REFLECTORS SHOWING EFFECTS OF CONSTANT RANGE-FREQUENCY OFFSET

FIGURE 31. IMAGE OF "M" SHOWING EFFECTS OF CONSTANT RANGE-FREQUENCY OFFSET

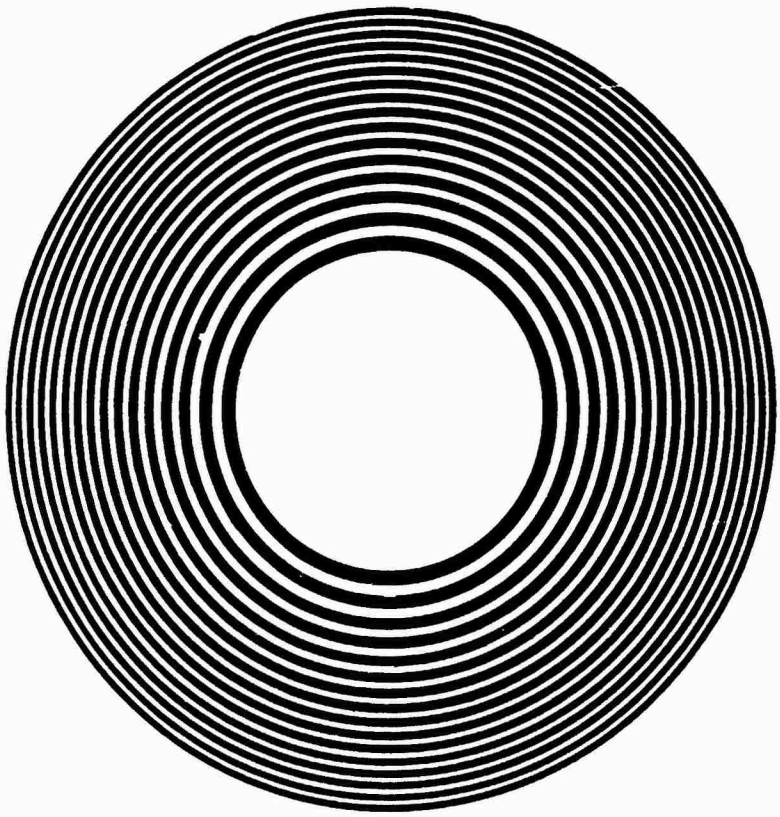

FIGURE 32. LINEAR FM RANGE OFFSET SIGNAL RECORDED IN A POLAR FORMAT

For the case of a constant range-frequency offset (Section 5.1), we found that the two conjugate terms of the Fourier transform of the recorded signal could be separated, but a phase error compensator in the optical processor was necessary. In the present case, we have a quadratic phase error which can be easily handled by a focus adjustment of the processor.

This technique has not yet been experimentally investigated. However, it appears to be a good approach for polar format recording systems used with the RADC Wideband Pulse Compression Radar.

The recorded signal $s_p(r_F, \phi_F)$ with a linear FM range offset is

$$s_p(r_F, \phi_F) = T_b + G \exp(j\psi_2) + G^* \exp(-j\psi_2) \tag{34}$$

where G is the Fourier transform of the reflectivity density $\sigma(r_o, \phi_o)$ as defined previously in Eq. (32).

The phase error ψ_2 can be shown to be

$$\psi_2 = \frac{2\pi r_F f_o}{v_s} + \left(\frac{\gamma_1 - \gamma_2}{2}\right)\left(\frac{r_F}{v_s} - \frac{2\pi f_c}{\gamma_1}\right)^2 \tag{35}$$

where γ_1 = chirp rate of the transmitted signal

γ_2 = chirp rate of the reference signal

f_c = carrier frequency of the video signal

If $\gamma_1 = \gamma_2$, the phase error given by Eq. (35) reduces to ψ_1, which is the phase error for the constant range frequency offset case in Eq. (30).

If $\gamma_1 \neq \gamma_2$ and the carrier frequency is chosen to be

$$f_o = \left(1 - \frac{\gamma_2}{\gamma_1}\right) f_c \tag{36}$$

then the phase error becomes

$$\psi_2 = \frac{\gamma_1 - \gamma_2}{2v_s^2} r_F^2 + \frac{2\pi^2 f_c^2}{\gamma_1^2}(\gamma_1 - \gamma_2) \tag{37}$$

The second term of Eq. (37) is a constant and therefore of no concern.

Since the remaining quadratic phase error appears with a different sign in the second and third terms of Eq. (34), the two conjugate images obtained by Fourier transforming the recorded signal $S(r_F, \phi_F)$ will focus in different planes. One image will focus in front of the usual Fourier transform plane of the processing lens and the other behind the Fourier transform plane. The important point is that with this type of offset a well focused image can be obtained by simple Fourier transformation of the recorded signal with no phase error compensation plates required.

It is necessary, however, to restrict the size of the coherent processing aperture in order to avoid contamination of the desired image with a noisy background resulting from the out-of-focus conjugate image.

5.3. POLAR OFFSET

A frequency offset technique designed especially for polar recording format systems involves the use of both time-varying range and cross-range (Doppler) frequency offsets. For brevity, this particular type of frequency offset is called polar offset.

Polar offset is implemented by sinusoidally modulating the frequency and the phase of the video signal in such a way that the recorded signal associated with the center of target rotation is a linear grating (see Fig. 33). That is, we introduce both range and cross-range frequency offsets which vary sinusoidally (90° out of phase) at the rotation rate of the recording material. For example, in the upper right portion of the recording shown in Fig. 33, the range-frequency offset is maximum and there is no cross range-frequency offset, while at the lower right, we have only cross-range frequency offset. The fact that the resulting recorded offset function is a linear grating implies that simple Fourier transform processing will produce an unambiguous image of a rotating object with no phase error compensation required. Furthermore, in contrast to the previous offset techniques, coherent processing can be performed over a full 360° of object rotation.

A polar offset can be implemented by mixing the signal received from the rotating object (Eq. 14) with a reference signal of the form

$$Z(t) = \cos\left\{2\pi f_c\left[t - \frac{2\rho_a(t)}{c} - \Delta(t)\right] + \frac{\gamma}{2}\left[t - nT - \frac{2\rho_a(t)}{c}\right]^2\right\} \tag{38}$$

where

$$\Delta(t) = \frac{2M}{c}\sin(\Omega t + \Phi)$$

After recording the resulting video signal in a polar format we obtain

$$s_p(r_F, \phi_F) = T_b + \iint B(r_F)\sigma(\rho_o, \phi_o)\cos\left\{\frac{2\gamma}{cv_s} r_F[\rho_o\cos(\phi_o - \phi_F) - M\cos(\phi - \phi_F]\right\}\rho_o d\rho_o d\phi_o \tag{39}$$

or expressed in rectangular coordinates

$$s_r(x_F, y_F) = S_b + \iint B(x_F, y_F)\tilde{\sigma}(x_o, y_o)\cos\left\{\frac{2\gamma}{cv_s}\cdot[x_F(x_o - x_a) + y_F(y_o - y_a)]\right\}dx_o dy_o$$

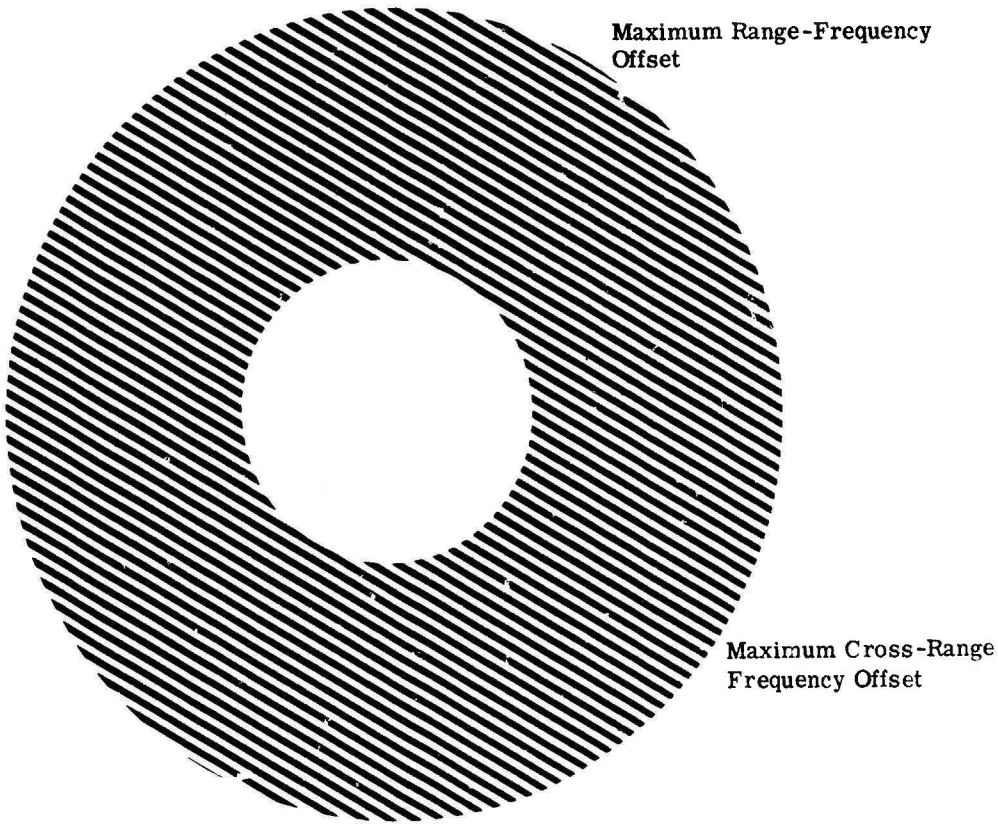

FIGURE 33. POLAR FREQUENCY-OFFSET SIGNAL

where $x_a = M \cos \Phi$

$y_a = M \sin \Phi$

Each point scatterer is recorded as a linear grating with x_F and y_F coordinate frequency components proportional to $(x_o - x_a)$ and $(y_o - y_a)$ respectively.

The constant M determines the spatial frequency of the resulting offset grating; its value should be chosen to be larger than the expected radius of the rotating object in order to separate the conjugate images. The relative angular orientation of the offset grating is determined by Φ and can be chosen arbitrarily. The same type of receiver instrumentation for removing the effects of $\rho_a(t)$ from the received signal can also be used to introduce a polar offset.

An important point to note is that the form of Eq. (38) is the same as that of a signal received from a point with polar coordinates (M, Φ) on a rotating object. Therefore, a straightforward way to implement a polar offset is to use the return from a bright, prominent point on the object as a reference signal. In prominent point processing, the total signal received from the rotating object is simply envelope detected before being recorded on film and optically processed in the usual way. No local oscillator is used. If the object possesses a scattering point whose return is much stronger than the returns from other points on the object, the recorded signal corresponding to the composite return can be shown to be approximately the same as that given by Eq. (40). The coordinates (x_a, y_a) represent the initial location of the prominent scattering point. In situations where prominent point processing is applicable, one can obtain an image of a rotating object even if the radar does not have pulse-to-pulse coherence and even if gross object motion is ignored since the object provides its own coherent reference.

Some prominent point processing experiments were performed with the rotating platform facility to demonstrate the technique. Simple arrays of corner reflectors as well as a large cross-section reference corner were placed on the rotating platform. For these experiments the system shown in Fig. 10 was modified by substituting a simple diode detector receiver. The imagery of a three corner-reflector array obtained by using this receiver and the polar format recorder is essentially the same as that shown in Fig. 15(b). The primary difference is that the separation of the two conjugate images is determined by the distance between the prominent point and the object and is independent of the center of rotation. These experiments not only demonstrated prominent point processing but also verified the usefulness of the polar offset technique.

6
REAL-TIME OPTICAL PROCESSING

Real-time optical processing systems are generally comprised of an input transducer, processing optics, and a display screen. A time-varying signal to be processed optically must be entered at the input plane of the processor as a space varying (spatial) signal. The spatial input is then read into the processor simply by illumination with an expanded coherent light beam, and the readout light beam wavefront is modulated by the spatial signal. Real-time operation requires that the conversion to a spatial signal and the optical readout take place with insignificant delay. A real-time optical transducer is a device which serves this purpose. Recall that for the data processing experiments described in previous sections, photographic film served as a non-real-time transducer. Real-time transducer considerations relative to optical processing of rotating-object data will be discussed further in the following sections. The processing optics and the output viewing implementation have been covered in previous sections and inherently afford real-time operation.

6.1. THERMOPLASTIC TRANSDUCER

Electron beam writing on a deformable thermoplastic is the real-time, reusable, data storage method being evaluated for use in a real-time transducer. The thermoplastic transducer comprises: (1) a small evacuated housing containing the writing electron gun and thermoplastic storage medium; and (2) electronics for electron beam control and thermoplastic temperature control.

An input time-varying signal is written onto the thermoplastic as a surface charge using a scanned electron beam as depicted by Fig. 34(a). The charge deposited by the writing beam can be made to vary in proportion to the input signal in several ways; here, the beam current is directly modulated by controlling the electron gun grid-to-cathode voltage with the input signal.

The storage medium is comprised of a thin thermoplastic (TP) layer coated onto a glass substrate, with a thin transparent conductive coating between. The conductive film serves as a plane of constant electrical potential. It also serves as a means for electrical heating (I^2R) of the thermoplastic for rapid deformation development and data erasure.

Development and erasure of signals written in the thermoplastic are governed by the physical and electrical properties of the TP material and their change with temperature. The charge deposited on the thermoplastic surface during writing results in an electric field force between the TP surface and the equipotential plane at the conductive coating. This force acts to

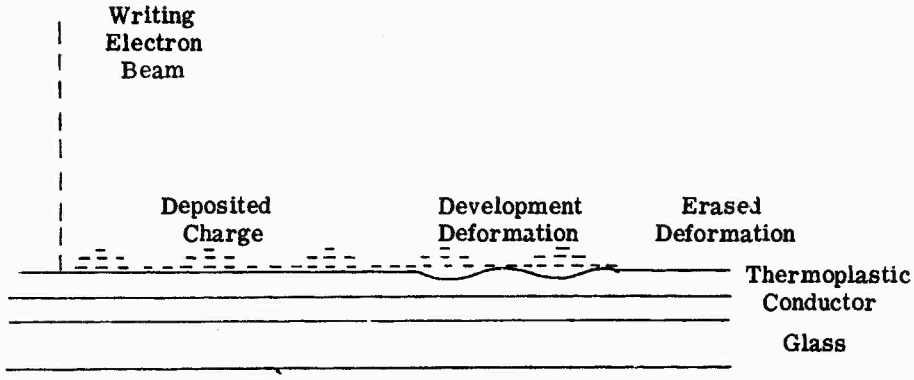

(a) Thermoplastic Data Storage

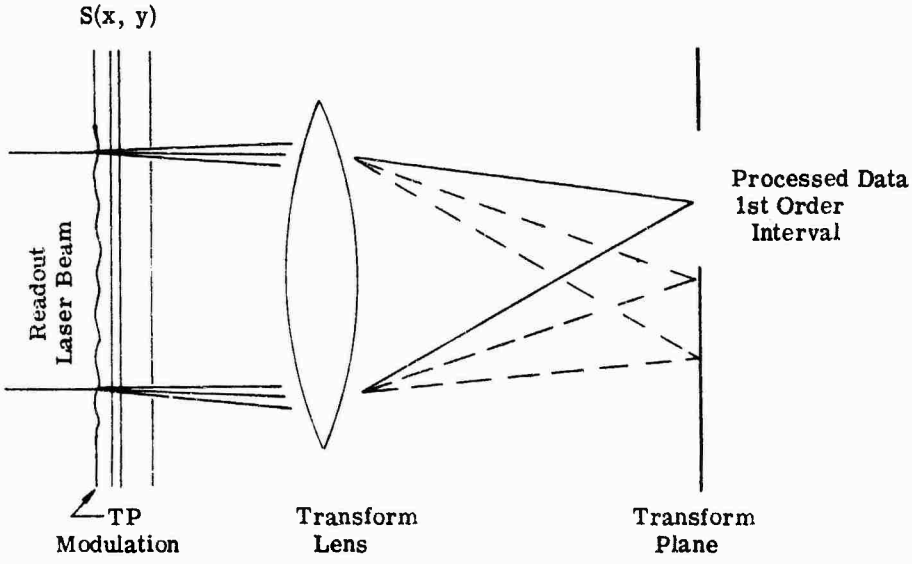

(b) Phase Readout for Data Processing

FIGURE 34. DATA STORAGE AND READOUT

deform the surface. Raising the thermoplastic temperature allows it to change from a solid to a rubber-like condition and then, with further temperature increase, to a liquid state. Deformation development can occur while the thermoplastic is in either of these softened states. The depth of the deformation will be limited by counteractive surface tension and viscoelastic forces. Erasure of signal deformations occurs when the surface charge is removed and the thermoplastic temperature is elevated so the plastic reaches a non-solid state and can be redistributed so as to form a smooth surface in response to the surface tension and viscoelastic restoring forces. In erasure, the written surface charge is removed by electrical conduction through the plastic to the conductive layer when the TP resistance is lowered by heating.

Data written in the thermoplastic modulator is read out with a laser beam expanded to illuminate the area over which stored signals of interest appear, as shown in Fig. 34(b). The sketch of 34(b) shows readout by transmission. (Reflective methods are also possible.) The complex transmittance of the thermoplastic modulator can be written as $T(x, y)e^{j\theta(x,y)}$ where T is the amplitude transmittance and θ the phase shift caused by the spatial modulator. Given an illuminating beam having a wavefront with uniform phase and constant amplitude over an aperture $A_o(x, y)$, the emergent beam $S(x, y)$ at the output side of the glass substrate will be of the form

$$S(x, y) = A_o(x, y)T(x, y)e^{j\theta(x,y)}$$

The amplitude transmittance will normally be constant, i.e., $T(x, y) = T_o$. Phase shift at the optical wavelength λ_o can be written as $\theta(x,y) = \{[2\pi(n - 1)/\lambda_o]d(x, y)\}\ \phi$ where d is surface deformation depth, n is the index of refraction of the thermoplastic, and ϕ is a phase shift caused by materials other than the thermoplastic, i.e., substrate and conductive coating. Thus the emergent phase-modulated readout beam is written as

$$S(x, y) = A_o(x, y)T_o e^{j\left[\frac{2\pi(n - 1)}{\lambda_o} d(x, y)\right]} e^{j\phi}$$

For example, consider the deformation d to be a one-dimensional sinusoid of spatial frequency ω_x

$$d = D_o + d \sin \omega_x X$$

as indicated in Fig. 34(b). As shown in Ref. [12] the expression for the phase-modulated readout beam can be written as

$$S(x) = A_o(x)T_o \exp\left\{j\left[\frac{2\pi(n - 1)}{\lambda_o} D \sin \omega_x x\right]\right\} = A_o(x)T_o \sum_{m=-\infty}^{\infty} J_m\left[\frac{2\pi(n - 1)}{\lambda_o} D\right] \exp jm\omega_x x$$

where we have ignored constant phase terms and $J_m[\ ]$ is a Bessel function of the first kind, order m. The indexing variable m takes on all integer values. Thus, there are plane waves $e^{jm\omega_x x}$ emanating from the modulator; each has a field amplitude $J_m\{[2\pi(n - 1)/\lambda]D\}$ and all come through the aperture $A_o(x)$.

If the modulator output is Fourier transformed optically as depicted in Fig. 34(b), the Fourier transform lens will focus each of the plane waves $e^{jm\omega_x x}$ into a small spot of light at the output transform plane of the lens. In this example each spot of light will have a shape or spatial distribution dependent on the size of the modulator aperture $A_o(x)$. The peak value of the light intensity of the focused spot will be proportional to $J_m^2\left\{\left[2\pi(n-1)/\lambda_o\right]D\right\}$ and thus depends upon the depth D of the sinusoidal deformation in the thermoplastic. The focused spot position will be directly proportional to the spatial frequency ω_x in the plane-wave expression $e^{jm\omega_x x}$. Data corresponding to one of the first orders ($m = \pm 1$) are usually used. The deformation depth D is then chosen to optimize the performance of the transducer in terms of linearity and efficiency.

6.2. PERFORMANCE INVESTIGATION

Our demountable electron gun recording facility was adapted for use as a thermoplastic transducer. In this effort special coating methods were developed for coating thermoplastic layers with good thickness uniformity and good optical quality; in addition, provisions for data writing, readout, and erasure were incorporated. (The major portion of this tranducer effort was sponsored under a separate contract and intended for different applications.) Transducer performance results important to satellite-imaging applications are described below.

The recording and coherent optical readout arrangement used to assess transducer performance is shown in Fig. 35. The collimated readout laser beam of variable diameter (3 mm to 50 mm) passes through the side entrance window of the TP transducer, reflects off an internal mirror to illuminate the TP surface, and passes through the TP and its substrate at an angle of 30^o from the surface normal. The emergent beam is phase-modulated by the recorded data and then passes through the Fourier transform lens. The output transform plane is located about 250 mm from the output surface of the lens. The light intensity distribution was observed both at the transform plane and also after magnification. Magnification was provided by a 4 mm focal length microscope objective lens with the magnified transform plane observed at about 1200 mm beyond the magnifying lens. The light intensity distribution in the transform plane, both unmagnified and magnified, was recorded on Polaroid film.

Electron beam writing was done with an unmodulated, 35 × 35 mm square raster at a selectable scan line repetition rate and a selectable number of lines per raster. Pulse modulation along each scan line was also accomplished. In this way either one- or two-dimensional gratings could be recorded to simulate radar data corresponding to either one- or two-point scatterers on a rotating object.

To adequately evaluate transducer feasibility in a future real-time optical processing system, modulation rates as high as 10 MHz were used. This rate exceeds the video bandwidths of both the ERIM Rotating Platform Radar and the RADC Wideband Pulse Compression Radar.

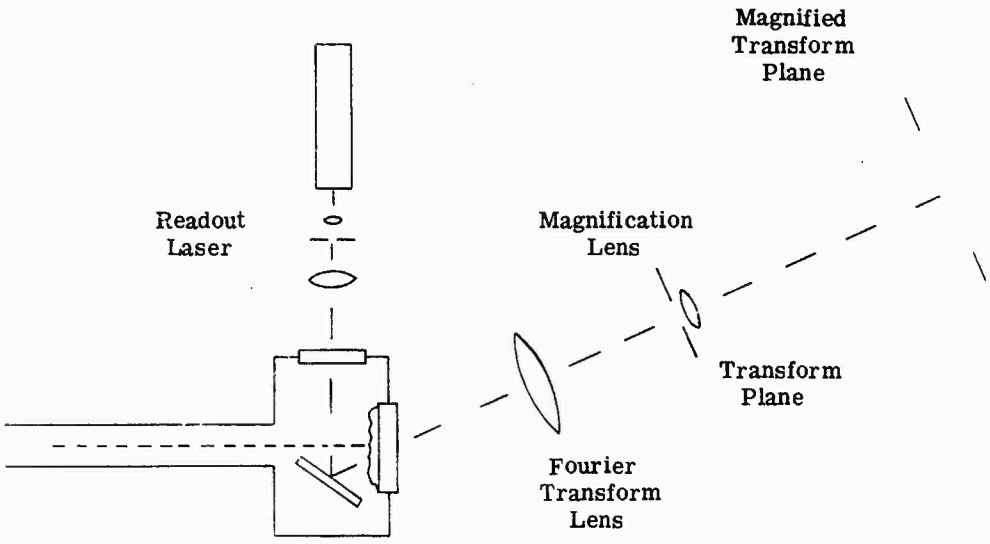

FIGURE 35. REAL-TIME TRANSDUCER FOR EXPERIMENTAL RECORDING USING ELECTRON BEAM WRITING AND COHERENT LIGHT BEAM READOUT

The spatial frequencies of the test recordings were chosen sufficiently high so that the number of resolvable recorded elements within the processing aperture would exceed the number of range and cross-range resolution cells required to adequately image a satellite (typically on the order of 100 × 100 cells).

The TP temperature was held constant with a fixed heater voltage V_c = 16.5 Vdc; this resulted in a temperature T_{po} = 45°C at the center of the outside surface of the TP substrate. The recording procedure typically consisted of writing a single raster (one exposure), allowing the deformation to develop, and then erasing while constant TP heater temperature was continuously maintained. At the constant TP temperature (and without application of a heat pulse for increased speed of development or erasure) the recording deformations developed in about 10 seconds and erased in about 600 seconds. With pulsed heating superimposed on a bias temperature level, development and erasure in less than a second can be realized.

Test recording was done on a TP coating about 5 μm thick which was coated over a 50 × 50 mm square by the gravity settled method. A quartz substrate with a tin oxide coating measuring 50 ohms edge-to-edge was used. The TP coating uniformity on this substrate prior to recording is indicated by its interferogram in Fig. 36.

Using the transducer and optical processing arrangement of Fig. 35, simple grating-type test signals were written onto the thermoplastic and then examined at the Fourier transform output plane. Examples of the light distribution in the transform plane are shown in Figs. 37 through 40. Figure 37(a) depicts the single focused spot of light which results when no data has been written on the TP and its surface is smooth. The distribution of Fig. 37(b) shows the center or zero order spot and a symmetric distribution of plus and minus order spots in the transform plane resulting from a 35 × 35 mm raster (one-dimensional grating) of 500 lines on the TP. The presence of orders as high as order six would not occur in the eventual mode of operation of the transducer and results here from the intentionally high level of exposure (three superimposed exposures). In addition, the effects of an extraneous modulation can be seen in Fig. 37(b) as evidenced by the very low intensity light distribution around the zero order caused by optical reflections in the test setup. Figure 37(c) shows the transform plane distribution resulting from a 35 × 35 mm raster containing 1000 lines written with a single exposure. In Fig. 37(d) is the transform plane for a two-dimensional crossed grating having 500 lines in one direction and 800 lines in the other. Figure 37(e) is a magnified Schlieren image of a 500-line raster recording.

To examine optical quality of the real-time transducer, a magnification of an individual order or spot in the transform plane is informative. For a given illuminated data aperture we look for evidence of diffraction-limited performance. A magnified version of the zero-order or first-order transform plane spots is given in Figs. 38 through 40. In Fig. 38 is the magnified light intensity distribution of the transform plane when the TP and substrate are not present. Essentially diffraction-limited performance can be seen for both the 12 mm and 25 mm diameter

FIGURE 36. MACH-ZEHNDER INTERFEROGRAM OF TYPE BO THERMOPLASTIC-COATED QUARTZ/TIN OXIDE SUBSTRATE

(a) No Recording, Smooth TP Film

(b) Raster Recording, 500 Lines

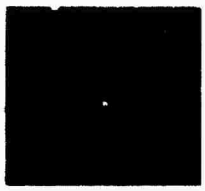

(c) Raster Recording, 1000 Lines

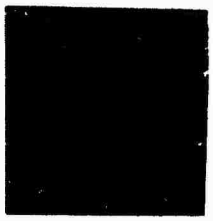

(d) Raster Recording, 500 Lines, 800 Pulses Per Line

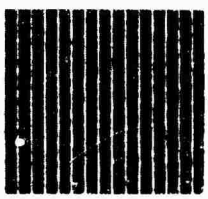

(e) Schlieren Image of 500 Line Raster

FIGURE 37. TRANSFORM PLANE LIGHT INTENSITY DISTRIBUTION FOR VARIOUS TP RECORDINGS

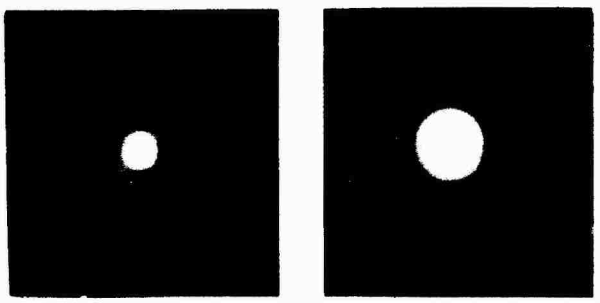

FIGURE 38. MAGNIFIED ZERO ORDER SPOT: TP PLATE NOT PRESENT IN TRANSDUCER

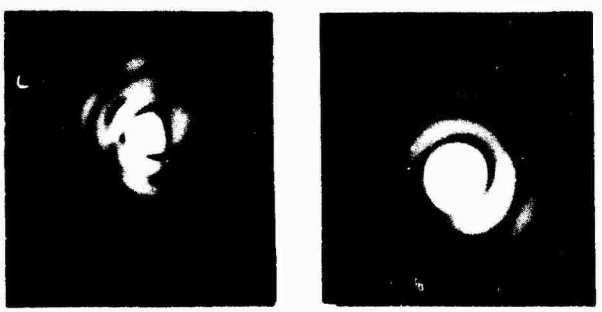

FIGURE 39. MAGNIFIED ZERO ORDER SPOT: WITH TP PLATE INSTALLED BUT NO RECORDING ON TP

FIGURE 40. MAGNIFIED FIRST ORDER SPOT: TP PLATE WITH 500 LINES IN 35 × 35 mm RASTER

25 mm 12 mm

Aperture Diameter

readout beams. This spot distribution represents the transducer impulse response without the recording plate. For the case where the TP-coated plate is installed but not written upon, the resultant magnified zero order spot (Fig. 39) again indicates good optical quality or good spatial impulse response for the transducer. Analogous data for the first-order spot obtained by Fourier transformation of the light diffracted by a 35 × 35 mm raster containing 500 lines is shown in Fig. 40. The results shown for the 12 mm and 25 mm diameter illumination aperture of the 35 × 35 mm raster are of good quality and nearly diffraction limited.

In summary, the thermoplastic data storage technique has been shown to have a sound potential for application as a real-time transducer for optical processing of rotating object radar data. The experimental transducer facility demonstrated a video bandwidth of at least 10 MHz, data storage with good optical quality over apertures containing at least 400 × 400 resolvable recorded elements, and rapid development and erasure.

7
CONCLUSIONS AND RECOMMENDATIONS

(C)Recording radar data in a polar format for subsequent optical processing has been shown to provide a simple and practical way to obtain very fine resolution imagery of rotating objects. The usual resolution limitation of rotating-object radar imagery imposed by motion through resolution cells is removed by means of this technique. Imagery of test objects placed on a rotating platform demonstrated that resolution of nearly one radar wavelength could be achieved. Moreover, the use of a polar recording format provided a convenient way to optically process radar data over large angles of rotation to improve the shape recognition of specular objects.

The imagery shown in this report was obtained under controlled experimental conditions in which the rotation rates of the test objects were known and no gross translation effects were present. Therefore, future investigation should be directed toward optically processing actual satellite data—for example, data from the RADC Wideband Pulse Compression Radar.

Experiments have shown that the thermoplastic data storage technique has sound potential for use in a real-time optical processing system. It is recommended that a breadboard version of a real-time thermoplastic transducer utilizing a polar storage format be developed to investigate real-time optical processing of radar data from the ERIM Rotating Platform Radar Facility as well as from the RADC Wideband Pulse Compression Radar.

REFERENCES

1. J. V. Evans and T. Hagfors, Radar Astronomy, McGraw-Hill (1968)
2. W. M. Brown, "Synthetic Aperture Radar", IEEE Trans. on Aerospace and Elec. Systems, Vol. AES-3, p. 217 (1967)
3. E. N. Leith, "Quasi-Holographic Techniques in the Microwave Region", Proc. of IEEE, Vol. 59, p. 1305, (1971)
4. "Signal Processing Method and Analysis for Motion and Imaging" (U), Syracuse University Research Corp., RADC-TR-72-187 (1972) (Secret)
5. W. M. Brown and R. Fredricks, "Range-Doppler Imaging with Motion Through Resolution Cells," IEEE Trans. on Aerospace and Elec. Systems, Vol. AES-5, p. 236, (1969)
6. W. Carrara and R. Maes, "Optical Processing of SOI Radar Data" (U), Final Report RADC-TR-68-325, Willow Run Laboratories, The University of Michigan, Ann Arbor (1969) (Confidential)
7. W. M. Brown and R. Fredricks, "Optical Data Processing for SOI Radar and Related Problems" (U), Final Report 1058-8-P, Willow Run Laboratories, The University of Michigan, Ann Arbor (1968) (Secret)
8. E. L. Johansen, et al., "Rotating Target Imaging" (U), Report 37000-51-T, Willow Run Laboratories, The University of Michigan, Ann Arbor (In Publication)(Confidential)
9. J. W. Goodman, Introduction to Fourier Optics, McGraw-Hill, p. 68 (1968)
10. R. O. Harger, Synthetic Aperture Radar Systems: Theory and Design, Academic Press (1970)
11. W. J. Caputi and R. B. VanDeusen, "High Resolution Stretch Radar" (U), Tenth Annual Radar Symposium Record, Report 6400-11-X, The University of Michigan, Ann Arbor (1964)(Secret)
12. J. S. Zelenka, G. F. Adams, and C. D. Leonard, "Phase Recording of Coherent Radar Data" (U), Seventeenth Annual Radar Symposium Record, Report No. 04900-1-X(I), Willow Run Laboratories, The University of Michigan, Ann Arbor (1971) (Secret)

UNCLASSIFIED
Security Classification

DOCUMENT CONTROL DATA - R & D

(Security classification of title, body of abstract and indexing annotation must be entered when the overall report is classified)

1. ORIGINATING ACTIVITY (Corporate author) Environmental Research Institute of Michigan Radar and Optics Division P.O. Box 618, Ann Arbor, Michigan 48107	2a. REPORT SECURITY CLASSIFICATION CONFIDENTIAL 2b. GROUP GDS - 31 Dec 1979

3. REPORT TITLE
OPTICAL PROCESSING OF ROTATING-OBJECT RADAR DATA USING A POLAR RECORDING FORMAT (U)

4. DESCRIPTIVE NOTES (Type of report and inclusive dates)
Final Report covering 1 February 1972 through 1 February 1973

5. AUTHOR(S) (First name, middle initial, last name)
J. L. Walker
W. G. Carrara
I. Cindrich

6. REPORT DATE	7a. TOTAL NO. OF PAGES	7b. NO. OF REFS
May 1973	vii + 65	12

8a. CONTRACT OR GRANT NO. F30602-72-C-0062 new b. Job Order No: 45060176 c. d.	9a. ORIGINATOR'S REPORT NUMBER(S) 191400-1-F 9b. OTHER REPORT NO(S) (Any other numbers that may be assigned this report) RADC-TR-73-136

10. DISTRIBUTION STATEMENT
Distribution limited to U. S. Gov't agencies only; test and evaluation; May 1973. Other requests for this document must be referred to RADC (OCTS), GAFB, NY 13441.

11. SUPPLEMENTARY NOTES	12. SPONSORING MILITARY ACTIVITY
	Rome Air Development Center (OCTS) Griffiss Air Force Base, New York 13441

13. ABSTRACT

A new optical processing technique for producing fine resolution radar images of rotating objects has been investigated. The technique involves optically recording the radar data in an appropriate polar format to eliminate the usual image degradation caused by motion of object points through resolution cells.

Experiments were performed in which X-band radar data from various test objects placed on a rotating platform were recorded on photographic film in a polar format and optically processed. The resulting imagery demonstrated the fine resolution and object-shape recognition capability afforded by the use of the polar recording format.

The feasibility of using thermoplastic as a real-time storage medium for radar data was investigated. The thermoplastic data storage technique was shown to have sound potential for use in a real-time optical processing system for satellite imaging applications.

DD FORM 1 NOV 65 1473

UNCLASSIFIED
Security Classification

UNCLASSIFIED
Security Classification

14. KEY WORDS	LINK A		LINK B		LINK C	
	ROLE	WT	ROLE	WT	ROLE	WT
Optical Processing Radar Imaging Rotating Object Imaging Real-Time Processing						

UNCLASSIFIED
Security Classification

SAM--Griffiss AFB NY